Uppsala Universitet

Department of Physics and Astronomy

Master thesis, 30 credits

Quasicrystal nanowires in SNS-junctions

Author: Anna Sandberg

Supervisor: Patric Holmvall

Subject reader: Annica Black-Schaffer

Examiner: Andreas Korn

September 8, 2022

Abstract

Quasicrystals are systems that are ordered but not periodic. They do however still have long-range order and well-defined diffraction peaks. This leads to interesting properties, like critical states which are neither extended nor localized, and to topological invariants and edge states. We study how these peculiar properties impact superconductivity in an SNS-junction, by attaching superconducting leads to a quasicrystal nanowire. We choose to investigate proximitzed superconductivity in Fibonacci quasicrystals, since their normal state has been thoroughly studied and understood. Using the Bogoliubov-de Gennes method and solving the order parameter self-consistently, we calculate the proximity effect as well as the Josephson current. We find that quasicrystals can enhance the proximity effect and significantly enhance the Josephson currents.

Contents

1 Populärvetenskaplig sammanfattning

Kvasikristaller är system som är ordnade men som saknar periodicitet. Trots detta så är de ordnade över långa avstånd och har väldefinierade diffraktionsmönster. Detta ger upphov till intressanta egenskaper som skiljer sig från de hos kristallina, periodiska, material och amorfa, oordnade, material. Bland annat så kan de ha så kallade topologiska egenskaper, som gör materialets egenskaper robusta mot vissa sorters störningar. Detta är spännande eftersom denna sortens egenskaper annars bara går att finna i periodiska system av högre dimension. Ett exempel på kvasikristallina strukturer är Penrosemönster, se Figur 1. En endimensionell kvasikristall är Fibonacci-kvasikristallen, som baseras på Fibonaccis talföljd. Fibonaccis talföljd är en rekursiv talföljd där varje nytt tal är summan av de två föregående talen i talföljden. En Fibonacci-kvasikristall kan konstrueras på ett liknande sätt, där varje ny Fibonaccikedja bildas genom att sammanfoga de två föregående kedjorna.

I detta masterarbete undersöker vi hur kvasikristallers unika egenskaper samverkar med ett ordnat tillstånd så som supraledning. Supraledning är ett tillstånd som existerar i vissa material vid tillräckligt låga temperaturer och karaktäriseras av två fenomen. Det första fenomenet är perfekt elektrisk ledningsförmåga, vilket innebär att resistiviteten i materialet går ner till noll. Det andra fenomenet är perfekt diamagnetism, även kallat Meissnereffekten. Detta innebär att alla magnetfält kastas ut ur materialet.

Vi undersöker hur kvasikristallers speciella karaktärsdrag påverkar supraledningen i så kallade Josephsonövergångar, eller mer specifikt SNS-övergångar, hybridsystem som innehåller två supraledare med en normal metall emellan. Dessa utformas genom att fästa två supraledare på ändarna av en endimensionell Fibonaccikvasikristall. Vi studerar två fenomen som uppstår i SNS-övergångar, proximitetseffekten samt Josephsonströmmen. Proximitetseffekten beskriver hur mycket supraledningen ”läcker in” in normaldelen från supraledaren. I SNS-övergångar kan man även ha så kallade Josephsonströmmar, vilket är superströmmar från den ena supraledaren till den andra genom normaldelen, trots att normaldelen i sig inte är supraledande. Genom att göra numeriska beräkningar fann vi att kvasikristaller kan förbättra proximitetseffekten något, men framför allt så kan de märkbart förbättra Josephsonströmmen.

2 Introduction

Quasicrystals are ordered structures that lack periodicity. They fall somewhere in the realm between periodic crystals and disordered amorphous materials, which gives them interesting properties, some of which can otherwise only be found in periodic systems of higher dimension. Since they first were discovered in the 1980s, quasicrystals have gained a lot of research interest mainly because of their electronic properties. Mathematicians discovered aperiodic tilings already in the 1960s, with the Penrose tilings [1] being some of the more well-known, but it took 20 more years until they made their way into crystallography. In the beginning of the 1980s, Alan L. Mackay [2] made predictions for the crystallography of quasicrystals and the first experimental findings of quasicrystals were made by Dan Shechtman [3]. In 2011, Shechtman was awarded the Nobel Prize in Chemistry for this discovery.

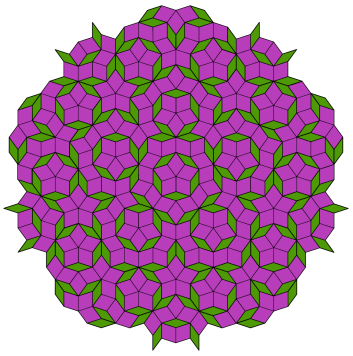

Figure 1: A Penrose tiling

With advances in nanotechnology, it is becoming more and more feasible to fabricate and study quasicrystals, even with single-atom precision [4]. Since they first were discovered, the normal state of quasicrystals have been thoroughly studied, while the impact of ordered states in quasicrystals is not as well understood. Although efforts have been made to study superconductivity in quasicrystals, very few experiments have been able to detect intrinsic superconductivity in quasicrystals [5]. An adjacent research area that has remained relatively unexplored is that of proximitized superconductivity in quasicrystals. A theoretical study made on superconductor-quasicrystal hybrid rings [6], found that the quasiperiodicity in some cases could enhance the proximity effect, compared to a periodic chain.

This master thesis aims to expand on that work by studying quasicrystal SNS-junctions, in which we not only verify qualitatively the results for the proximity effect but also study the Josephson current. SNS-junctions are hybrid systems consisting of two superconductors with a normal metal in between, and have many applications, e.g. in SQUIDs and quantum computing. In this thesis we replace the usually periodic normal metal with a Fibonacci quasicrystal. We find that although the proximity effect can only be seen to be somewhat larger for certain quasiperiodic chains, the Josephson current can be significantly enhanced by quasiperiodicity, in particular when the transmission between the superconductors and the quasicrystal is not perfect.

This thesis is outlined as follows: Theory on quasicrystals, with the 1D Fibonacci quasicrystal in focus, is discussed in Section 3. Theory on superconductivity and the Bogoliuobov-de Gennes method are reviewed in Section 4, as well as some details around how to solve the self-consistent gap equation. Section 5 discusses the physics of SNS-junctions, the proximity effect and Josephson currents. The results are presented and discussed in Section 6 and lastly we have Section 7 with conclusions and outlook.

3 Quasicrystals

Quasicrystals are structures that are ordered, but unlike regular crystals, they lack translational symmetry. They do however still exhibit discrete rotational symmetry, long-range order and scale invariance. The rotational symmetries found in quasicrystals differ from those found in crystals, as they prohibit periodicity in the material. Similarly to periodic crystals, and unlike amorphous materials, quasicrystalline materials have sharp diffraction patterns made up of Bragg peaks. For a periodic crystal of the spatial dimension d, the number of reciprocal lattice vectors that are required to index the Bragg peaks are equal to d. For a quasicrystal however, the number of reciprocal lattice vectors D needed to index the Bragg peaks is larger than the spatial dimension d [7].

Quasicrystals exhibit many different interesting behaviours such as multifractal energy spectra and critical states, i.e. states that are neither extended nor localized. They also provide a platform to study topology and edge states, as they are topological invariants [7].

In this thesis we study the one-dimensional Fibonacci quasicrystal, as it is one of the most researched and well-understood quasiperiodic systems. Sections 3.1 and 3.1.1 describe ways in which a Fibonacci chain can be constructed, while Section 3.1.2 details a tight-binding Fibonacci model and Section 3.1.3 shortly discusses the topological properties of the Fibonacci quasicrystal.

3.1 The Fibonacci chain

One example of a 1D quasicrystal is the Fibonacci chain. The Fibonacci numbers form a sequence in which each Fibonacci number, F_n, is the sum of the two previous numbers in the sequence, i.e. following the recursion relation $F_n = F_{n-1} + F_{n-2}$, with $F_0 = 0$ and $F_1 = 1$. The Fibonacci chain can be generated in a similar way, but instead we use the letters A and B, and concatenate the two previous chains to form the next chain, C_n, in the following way [7]:

$$C_n = C_{n-1} \oplus C_{n-2} \tag{1}$$

with $C_0 = B$ and $C_1 = A$. C_n is a finite approximant of an infinite Fibonacci chain, which can be obtained by letting $n \to \infty$. The length of the n:th approximant is equal to the Fibonacci number F_n. The first few Fibonacci approximants can be seen in Tab. 1 and a physical interpretation of such an approximant can be seen in Fig. 2. If one takes the ratio between two consecutive Fibonacci numbers and then let $n \to \infty$, the ratio will go towards the golden mean, $\tau = (1 + \sqrt{5})/2$ [7]:

$$\begin{aligned} \frac{F_{n-1}}{F_{n-2}} &= \tau_n, \\ \lim_{n\to\infty} \tau_n &= \tau, \end{aligned} \tag{2}$$

n	C_n	F_n
0	B	1
1	A	1
2	AB	2
3	ABA	3
4	ABAAB	5
5	ABAABABA	8
6	ABAABABAABAAB	13
7	ABAABABAABAABABAABABA	21

Table 1: The first eight Fibonacci approximants. Each new chain C_n is constructed by concatenating the previous two chains, C_{n-1} and C_{n-2}. The length of the n:th approximant C_n is equal to the Fibonacci number F_n.

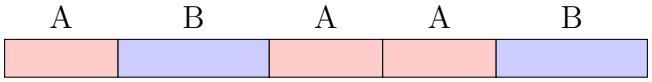

Figure 2: The 4:th Fibonacci approximant. In a physical system, the quasiperiodicity can be realised by for example having two different distances between the atoms in a lattice. Here A corresponds to the shorter distance (red) and B corresponds to the longer distance (blue).

with τ_n being rational approximants of the golden mean, τ.

3.1.1 The characteristic function

Another way of constructing a Fibonacci chain is using the characteristic function [7], [8], where the j:th letter of the chain is given by

$$\chi_j = \mathrm{sgn}[\cos\big(2\pi j\tau^{-1} + \phi_0\big) - \cos\big(\pi\tau^{-1}\big)], \tag{3}$$

where $j = 1, 2, 3, ...$ and $\chi_j = -1$ corresponds to the letter A and $\chi_j = 1$ to the letter B. For the Fibonacci chain, $\tau = (1 + \sqrt{5})/2$ is the golden mean and $\phi_0 = \pi\tau^{-1}$ [6]. If the chain is ended at the length F_n, it will correspond to the n:th Fibonacci approximant C_n. The advantage of constructing the Fibonacci chain in this way is that ϕ_0 can be replaced by $0 \leq \varphi < 2\pi$, and as φ is varied *phason* flips occur, always one flip at a time. By varying the phason angle φ one can then generate a family of $(F_n + 1)$ chains of length F_n. From here on out we will use

$$\chi_j = \mathrm{sgn}[\cos\big(2\pi j\tau^{-1} + \varphi\big) - \cos\big(\pi\tau^{-1}\big)], \tag{4}$$

with the following parametrization $\varphi = (\phi - c_n)\ mod\ 2\pi$, where $c_n = (F_n + 1)\pi\tau^{-1}$. Figure 3 illustrates how the phason flips occur in the chain.

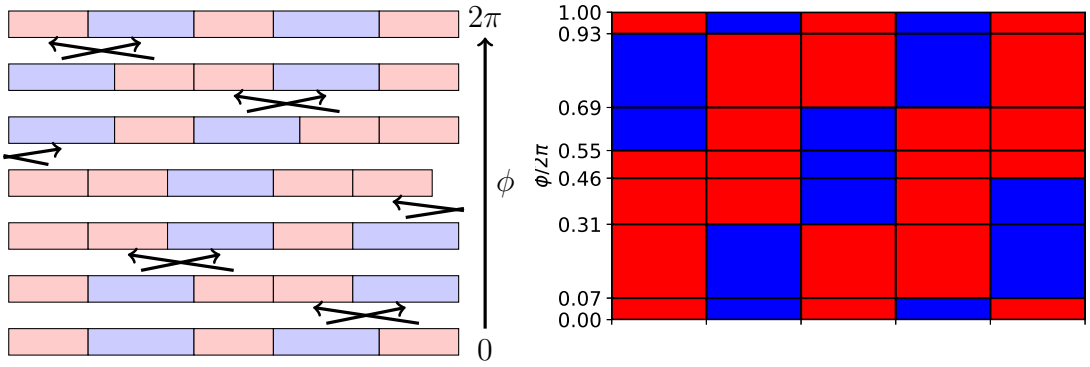

Figure 3: Phason flips in the 4:th Fibonacci approximant, red corresponds to the letter A and blue to the letter B. As the phason angle ϕ is varied single flips arise, altering the chain with a periodicity of 2π (left). Illustration of how the chains look corresponding to different values of ϕ (right).

3.1.2 Tight-binding Fibonacci models

Tight-binding models are often used in condensed matter physics, e.g. for quasicrystals, or as is discussed in Section 4.1.1, for superconductors. The theory of tight-binding models is explained further in that section. Fibonacci chains are often studied using tight-binding models of the following form

$$H = \sum_n \epsilon_n c_n^\dagger c_n - (t_n c_{n+1}^\dagger c_n + H.c.), \tag{5}$$

where ϵ_n is the on-site energy at the n:th site and t_n is the hopping between sites n and $n+1$. The *modulations*, i.e. the variations of A and B in the chain, described previously can be incorporated into the tight-binding Hamiltonian in different ways. The two simplest Fibonacci models are the *diagonal Fibonacci model*, in which the modulations are placed in the on-site energies ϵ_n, and the *off-diagonal Fibonacci model*, in which the quasiperiodicity is put in the hopping energies t_n [7]. In this report we focus on the latter case, letting the hopping energies t_n take one of two values t_A and t_B according to the modulations of a Fibonacci chain. The on-site energies ϵ_n are taken to be constant, i.e. $\epsilon_n = \epsilon$, which allows us to drop the on-site energy term and leaves us with the following Hamiltonian:

$$H = -\sum_n t_n c_{n+1}^\dagger c_n + H.c. \tag{6}$$

By using t_B as the unit of energy we are left with the ratio $\rho = t_A/t_B$, where $\rho = 1$ is the periodic case, as the only parameter, allowing us to adiabatically switch on the quasiperiodicity. One can then either just look at a single Fibonacci approximant C_n, or construct a quasiperiodic chain by using the approximant C_n as a sublattice, and then repeat the sublattice N number of times to get the whole lattice.

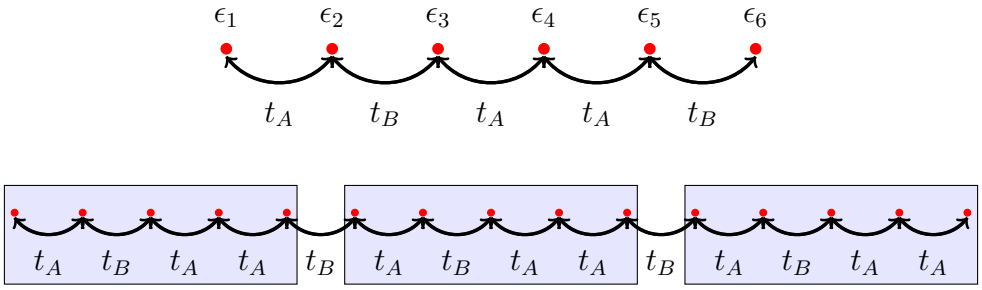

Figure 4: The upper figure illustrates the lattice for the 4:th Fibonacci approximant. For some systems it can be relevant to use the approximant as a sublattice in a longer chain. Then the last hopping of the approximant chain couples to the subsequent approximant sublattice. This is illustrated in the lower figure.

Such structures, with repeated sublattices of a Fibonacci approximant, occur naturally in 3-dimensional icosahedral and dodecagonal quasicrystals. This has for example been shown in experiments using STM imaging of copper adatoms deposited on an icosahedral AlPdMn quasicrystal [9]. Figure 4 illustrates the lattice for the 4:th Fibonacci approximant.

3.1.3 The gap labeling theorem and topological indices

As one goes from a periodic system to a quasiperiodic system, gaps will open up in the energy spectra. One of the few known exact results for the electronic properties of quasicrystals is the gap labeling theorem [10], which gives constraints on what values the *integrated density of states* (IDOS) can take within a spectral gap. The IDOS at an energy E is defined as the fraction of the energy states which are below the energy E, or in other words, ids(E) is calculated by integrating the normalized density of states up to the energy E.

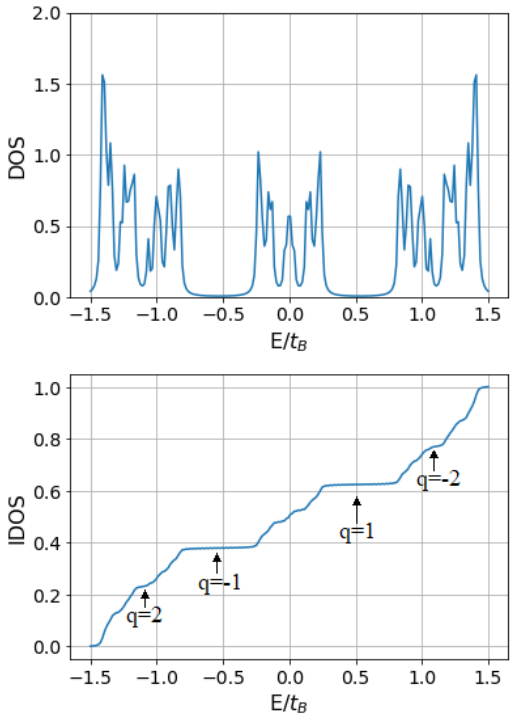

Figure 5: Density of states (upper) and integrated density of states (lower) for Fibonacci approximant $n = 10$, with 90 sites and $t_A/t_B = 0.5$, with the largest gaps marked with their gap label q.

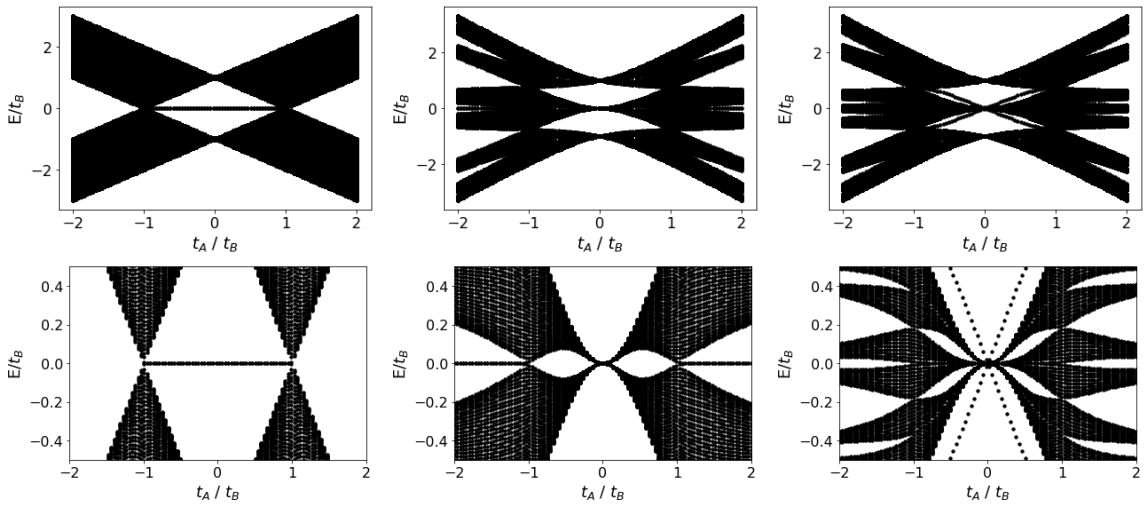

(a) $n = 2$ (b) $n = 5$ (c) $n = 8$

Figure 6: The energy spectra as a function of t_A/t_B for three different approximants, repeated so that the chains are of similar length for all three systems. The upper row displays the full spectra, while the lower row shows it zoomed in around $E = 0$. (a) The 2:nd approximant (repeated $N = 150$ times). (b) The 5:th approximant (repeated $N = 40$ times). (c) The 8:th approximant (repeated $N = 10$ times). As the modulation strength is increased/decreased from $|t_A/t_B| = 1$ (which corresponds to a periodic chain), the system becomes quasicrystalline and gaps open up in the energy spectra. In the zoomed in plots one may also note that there are flat bands at zero energy.

The definition of density of states and integrated density of states, and how these quantities are calculated using Bogoliubov-de Gennes formalism, is described in a later section, see Eq. (35) and Eq. (36).

In the spectral gap, the IDOS is constant, and this constant value is decided by the gap labeling theorem. For the special case of the Fibonacci chain the theorem states that [11]

$$\text{ids}(E \in gap) = \frac{q}{\tau_n} \mod 1 \tag{7}$$

where q is the gap label. It has been shown that this theorem applies not only in the quasiperiodic limit, i.e. when $n \to \infty$, but also to the approximants [11], with the caveat that some of the gaps in the approximants are *transient*, meaning they only appear for some of the approximants but do not exist for the full infinite Fibonacci chain. Other gaps are however *stable*, meaning they stay open in the quasiperiodic limit. It turns out that the transient gaps are always the ones with the highest gap label.

Incidentally, the gap label also has a physical meaning, as it is associated to a topo-

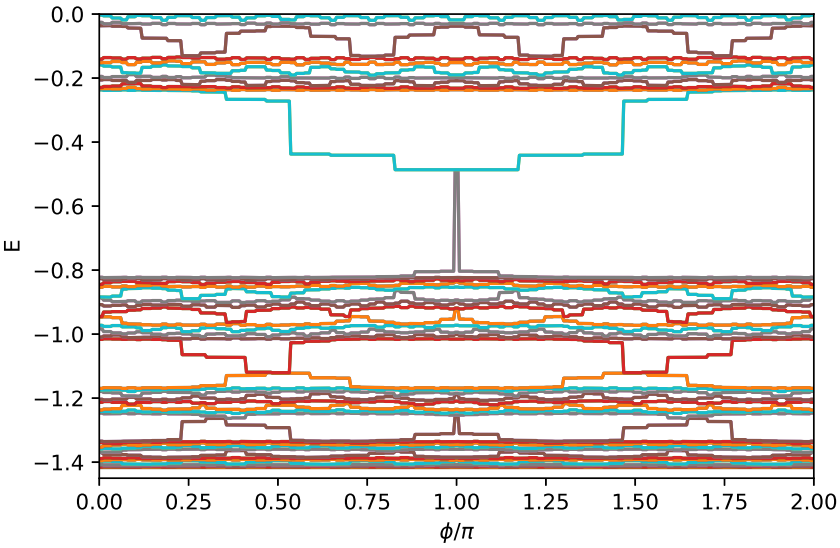

Figure 7: The lower part of the energy spectra as a function of the phason angle, for an open Fibonacci chain, $n = 10$, with 90 sites. The hopping ratio is set to $t_A/t_B = 0.5$. Each gap can be given a label, a winding number, that corresponds to the number of crossings over that gap.

logical quantity. Mappings have been done between the 1D Fibonacci quasicrystal and a 2D quantum Hall system [8], [12], that show that the gap label q is in fact a Chern winding number inherited from the parent 2D model. These edge modes are thus topologically protected against local perturbations, e.g. disorder, as long as the symmetry is preserved.

The Fibonacci model has been shown to be topologically equivalent to the Harper model [8], which in turn has been shown to be topologically nontrivial. In the Fibonacci crystal there will thus exist edge modes and these can be tuned by varying the phason angle ϕ, which we introduced in Eq. (4). As ϕ is varied the energy levels will remain flat until a phason flip occurs. The gap label q, which we now know is a Chern winding number, corresponds to the number of crossings over that gap. This can be seen in Fig. 7, which shows the lower part of the energy spectra as a function of the phason angle for the 10:th Fibonacci approximant. The phason angle then adds a second dimension to the system needed for the topological properties.

Experiments using polaritonic cavity modes have been able to confirm that the gap label q is a winding number [13], [14]. The experiments have studied the off-diagonal model by placing nearest neighbour cavities so that they would have either a strong or a weak coupling, depending on the distance to the neighbour. The modulation of the spacing would then follow a given Fibonacci sequence. According to the gap

label q of a certain gap, they then observed that the edge mode would cross the gap q times, verifying that the gap label q is a winding number. Whether q has a negative or positive sign depends on whether the crossing occurs from the lower to the upper edge of the gap or vice versa.

The topological properties of the Fibonacci model remain rather unexplored in solid state systems, as it requires the construction of an individual crystal for each value of the phason angle. It has been suggested that another way to probe the topological properties of the Fibonacci quasicrystal could be by measuring the charge density [15]. As it becomes easier to probe the topological properties of solid state Fibonacci quasicrystals, it is interesting to investigate how those properties interact with other ordered states, e.g. superconductivity.

3.1.4 Critical states

It has been shown that 1D quasiperiodic chains, e.g. Fibonacci chains, have critical states [16], i.e. states that are neither extended nor localized. Periodic crystals can be understood using Bloch states, $\psi_k(r) = u_k(r)e^{ikr}$, where u is a periodic function. This does however not apply to quasicrystals, but the wave function for $E = 0$ have an exact solution for the hopping model on 1D (and some 2D) quasiperiodic tilings, which employs a recursive construction. It was proposed that these quasiperiodic Hamiltonians have ground states ($E = 0$) that can be written as [17]

$$\psi(i) = C(i)e^{\kappa h(i)}, \tag{8}$$

where i is the site and κ is a real constant. $C(i)$ is a prefactor that depends on the local environment around the site i and h is the height field, which is the integral of a quasiperiodic function.

For the Fibonacci chain there are two independent $E = 0$ solutions, corresponding to two sublattices, which are equivalent in the limit of the infininte Fibonacci chain. We will now consider the solution for sites $i = 2m$. The solution can written on the recursive form [16]

$$\psi(m) = (-1)^m e^{\kappa h(m)}, \tag{9}$$

where $\kappa = \ln(t_A/t_B)$ and $h(m) = \sum_0^m A(j)$. The function $A(j)$ is defined by the configuration between sites j and $j + 1$,

$$A(j) = \begin{cases} +1 & \text{(AB)} \\ -1 & \text{(BA)} \\ 0 & \text{(AA).} \end{cases} \tag{10}$$

These states, in Eq. (9), can be shown to be critical states [16].

4 Superconductivity

Superconductivity is typically characterised by *perfect conductivity* and *perfect diamagnetism* [18]. In a normal metal the resistivity will decrease to a finite value as the temperature goes to zero. In a superconductor however, the resistivity drops to zero below a critical temperature T_c, see Fig. 8. The second thing that happens when the temperature goes below T_c is that the superconductor will expel any magnetic field from its interior. This is called the *Meissner effect* and is illustrated in Fig. 9. However, if one applies a strong enough magnetic field the superconducting state will be destroyed. Figure 10 shows the phase diagram for temperature T versus applied magnetic field H. Superconductors can be separated into two classes depending on their magnetic properties. *Type I superconductors* [18] exhibit a complete Meissner effect below the critical temperature T_c and the critical external magnetic field H_c, and for $H > H_c$, the superconductivity will disappear. *Type II superconductors* [18] will also exhibit a complete Meissner effect below a critical magnetic field $H_{c1} < H_c$, but will also have a phase with a mixed state for magnetic fields stronger than H_{c1} but weaker than H_{c2}. In this intermediate state, the magnetic field is no longer completely expelled from the material, but will feature a mix of normal and superconducting properties, with the formation of magnetic field vortices. For external magnetic fields stronger than H_{c2}, bulk superconductivity breaks down.

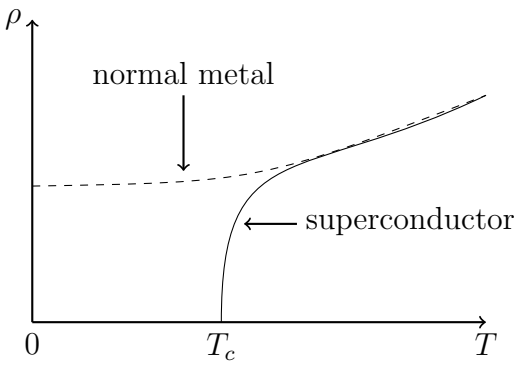

Figure 8: The first hallmark of superconductivity is perfect conductivity, i.e. that the resistivity drops to zero as the temperature goes below the critical temperature T_c.

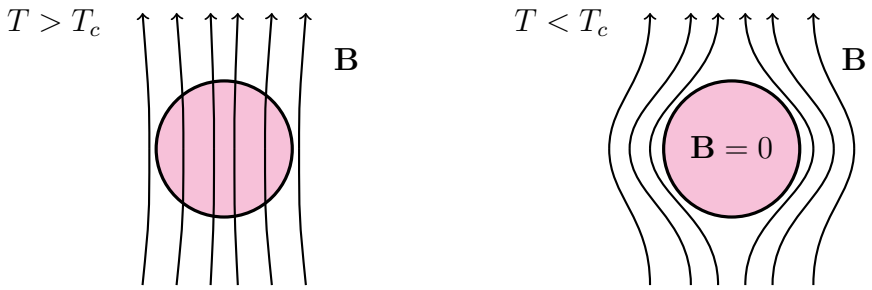

Figure 9: The second hallmark of superconductivity is perfect diamagnetism. As the temperature drops below the superconducting transition temperature T_c, any magnetic field inside the material is expelled.

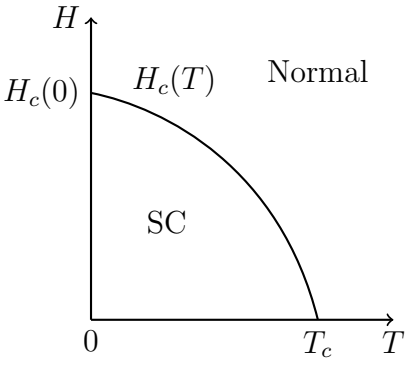

Figure 10: Phase diagram versus external magnetic field H and temperature T, for a Type I superconductor.

The first microscopic theory on superconductivity was BCS-theory [19], [20], which describes superconductivity as the condensation of Cooper pairs. Below a critical temperature, electrons at the Fermi surface form Cooper pairs, which are bosonic quasiparticles that are allowed (unlike fermions) to condensate. For the electrons to pair up, there has to be some attractive interaction between them, for example due to phonons, i.e. lattice vibrations. As the Cooper pairs form, a gap opens up at the Fermi surface, often referred to as the *superconducting gap*, Δ. It can also be referred to as the *pairing potential*, or the *order parameter*, since it provides a way of quantifying the superconductivity.

The superconducting gap can have different symmetries and structures depending on the material. Superconductors that have uniform gaps on the Fermi surface are said to have *s-wave* pairing symmetry, see Fig. 11. Another common type of superconductors are $d-wave$ superconductors.

Another way in which superconductors are categorised is by whether they are *conventional superconductors* or *unconventional superconductors*. There are two ways of defining what constitutes a conventional superconductor [21]. These often coincide but are not equivalent. The first is that a conventional superconductor has a superconducting state which breaks U(1) symmetry. The second one is that in a conventional superconductor, phonons are the main cause of the attractive interaction between the electrons.

In this thesis we are not interested in the magnetic properties, but rather the electronic properties of superconductivity. We study superconductivity using the Bogoliubov-de Gennes method, which is an extension to BCS-theory, and is detailed in Section 4.1. The order parameter was calculated self-consistently, for this a convergence accelerator was implemented, this is explained in Section 4.2.

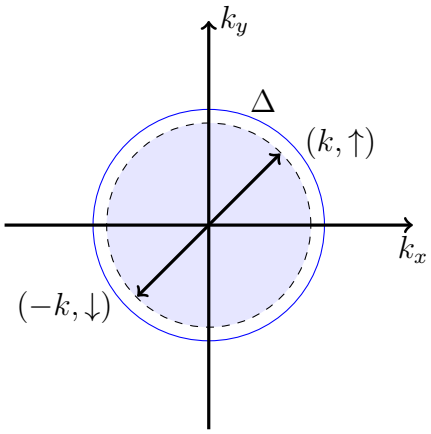

Figure 11: Electrons at the Fermi surface, with opposite spin and momentum, form Cooper pairs. This opens up the superconducting gap, Δ.

4.1 Bogoliubov-de Gennes theory of superconductivity

A method of studying superconductors is through the Bogoliubov-de Gennes (BdG) approach. The BdG equations can be derived in a continuum model as well as a tight-binding model. For this project we will use the tight-binding form of the BdG equations, which are derived in the following section.

4.1.1 Tight-binding derivation of the BdG equations

Tight-binding models are widely used in condensed matter physics to study many different phenomena. Here we will use one to derive the BdG equations for superconductivity in an s-wave superconductor. We begin from the single-particle part of the second-quantized Hamiltonian [22]:

$$H_0 = \iint d\mathbf{r}d\mathbf{r}'\psi^\dagger_\alpha(\mathbf{r})h_{\alpha\beta}(\mathbf{r},\mathbf{r}')\psi_\beta(\mathbf{r}'), \tag{11}$$

with spin-flip and non-local effects included in $h_{\alpha\beta}(\mathbf{r},\mathbf{r}')$. The field operators can be expressed in terms of the localized-state basis, as follows

$$\begin{aligned}\psi_\alpha(\mathbf{r}) &= \sum_i w(\mathbf{r}-\mathbf{R}_i)c_{i\alpha},\\ \psi^\dagger_\alpha(\mathbf{r}) &= \sum_i w^*(\mathbf{r}-\mathbf{R}_i)c^\dagger_{i\alpha},\end{aligned} \tag{12}$$

where the operators $c^\dagger_{i\alpha}$ and $c_{i\alpha}$ create and annihilate an electron at a site i with spin α. $w(\mathbf{r}-\mathbf{R}_i)$ is the localized orbital around the atomic site $\mathbf{R}_i$, and can be thought of as δ-functions centered at $\mathbf{R}_i$. By plugging Eq. (12) into the single-particle Hamiltonian we find [22]

$$\begin{aligned}H_0 &= \sum_{ij,\sigma\sigma'} c^\dagger_{i\sigma}h_{i\sigma,j\sigma'}c_{j\sigma}\\ &= -\sum_{i\neq j,\sigma\sigma'} t_{i\sigma,j\sigma'}c^\dagger_{i\sigma}c_{j\sigma'} + \sum_{i\sigma}\epsilon_i c^\dagger_{i\sigma}c_{i\sigma} + \sum_{i,\sigma\sigma'}\Omega_{i,\sigma\sigma'}c^\dagger_{i\sigma}c_{i\sigma'},\end{aligned} \tag{13}$$

where the first term is the kinetic energy from hopping between sites, the second term is the on-site single-particle energy, which can be included to account for disorder and inhomogenity such as single non-magnetic impurities, and the third term describes magnetic impurities. In this work we are not interested in the effects of such impurities, which means that the we will only be left with the hopping term, i.e.

$$H_0 = \sum_{ij,\sigma\sigma'} c^\dagger_{i\sigma}h_{i\sigma,j\sigma'}c_{j\sigma} = -\sum_{i\neq j,\sigma\sigma'} t_{i\sigma,j\sigma'}c^\dagger_{i\sigma}c_{j\sigma'}. \tag{14}$$

In order to get s-wave superconductivity we then add an attractive on-site electron-electron interaction with strength U ($U > 0$), getting the following Hamiltonian for superconductivity [22]

$$\mathscr{H} = \sum_{ij,\sigma\sigma'} c^\dagger_{i\sigma}\Big[h_{i\sigma,j\sigma'} - \mu\delta_{ij}\delta_{\sigma\sigma'}\Big]c_{j\sigma'} - U\sum_i n_{i\uparrow}n_{i\downarrow}, \tag{15}$$

with the chemical potential μ, which we include to regulate the mean number of particles, the number operator $n_{i\sigma} = c^\dagger_{i\sigma}c_{i\sigma}$, and $n_i = \sum_\sigma n_{i\sigma}$. Working with four field operators is rather complicated, however, the electron-electron interaction term can be simplified by doing the following *mean-field approximation* [22]:

$$c^\dagger_{i\uparrow}c^\dagger_{i\downarrow}c_{i\downarrow}c_{i\uparrow} \approx \langle c^\dagger_{i\uparrow}c^\dagger_{i\downarrow}\rangle c_{i\downarrow}c_{i\uparrow} + c^\dagger_{i\uparrow}c^\dagger_{i\downarrow}\langle c_{i\downarrow}c_{i\uparrow}\rangle - \langle c^\dagger_{i\uparrow}c^\dagger_{i\downarrow}\rangle\langle c_{i\downarrow}c_{i\uparrow}\rangle, \tag{16}$$

This is similar to what is done in Hartree-Fock, the difference here being that we pair annihilation operators together and creation operators together, instead of pairs of one annihilation operator and one creation operator. Plugging Eq. (16) into Eq. (15) we get the following

$$\begin{aligned}\mathscr{H} &= \sum_{ij,\sigma\sigma'} c^\dagger_{i\sigma}\tilde{h}_{i\sigma,j\sigma'}c_{j\sigma'} - U\sum_i c^\dagger_{i\uparrow}c^\dagger_{i\downarrow}c_{i\downarrow}c_{i\uparrow} \\ &\approx \sum_{ij,\sigma\sigma'} c^\dagger_{i\sigma}\tilde{h}_{i\sigma,j\sigma'}c_{j\sigma'} - U\sum_i(\langle c^\dagger_{i\uparrow}c^\dagger_{i\downarrow}\rangle c_{i\downarrow}c_{i\uparrow} + c^\dagger_{i\uparrow}c^\dagger_{i\downarrow}\langle c_{i\downarrow}c_{i\uparrow}\rangle - \langle c^\dagger_{i\uparrow}c^\dagger_{i\downarrow}\rangle\langle c_{i\downarrow}c_{i\uparrow}\rangle)\end{aligned} \tag{17}$$

where $\tilde{h}_{i\sigma,j\sigma'} = h_{i\sigma,j\sigma'} - \mu\delta_{ij}\delta_{\sigma\sigma'}$. The singlet-pairing potentials can be expressed as

$$\begin{aligned}\Delta_{ii} &= U\langle c_{i\downarrow}c_{i\uparrow}\rangle, \\ \Delta^*_{ii} &= U\langle c^\dagger_{i\uparrow}c^\dagger_{i\downarrow}\rangle,\end{aligned} \tag{18}$$

which leaves us with the following effective Hamiltonian,

$$\mathscr{H}_{eff} = \sum_{ij,\sigma\sigma'} c^\dagger_{i\sigma}\tilde{h}_{i\sigma,j\sigma'}c_{j\sigma'} - \sum_i\Big[\Delta_{ii}c^\dagger_{i\uparrow}c^\dagger_{i\downarrow} + \Delta^*_{ii}c_{i\downarrow}c_{i\uparrow}\Big] + E_{const}, \tag{19}$$

where $E_{const} = U\sum_i\langle c^\dagger_{i\uparrow}c^\dagger_{i\downarrow}\rangle\langle c_{i\downarrow}c_{i\uparrow}\rangle$. We have now gained a simpler, quadratic term for the electron-electron interaction, meanwhile we have also thrown it into a form that is approximative and does not conserve the particle number. Instead it contains terms that create or annihilate pairs of particles. This can be handled by using the chemical potential μ, which was introduced earlier, in order to fix the number of particles.

We then proceed by looking at the commutation relations for the creation and annihilation operators and the effective Hamiltonian. The commutation relation between

$c_{i\uparrow}$ and H_{eff} can be calculated as

$$\begin{aligned}[c_{i\uparrow}, \mathscr{H}_{eff}] &= c_{i\uparrow}\mathscr{H}_{eff} - \mathscr{H}_{eff}c_{i\uparrow} \\ &= \sum_{j,\sigma'} \tilde{h}_{i\uparrow,j\sigma'}c_{j\sigma'} + \Delta_{ii}c^{\dagger}_{i\downarrow}.\end{aligned} \tag{20}$$

Performing the same calculation for the remaining electron field operators we get the following commutation relations,

$$\begin{aligned}[c_{i\uparrow}, \mathscr{H}_{eff}] &= \sum_{j,\sigma'} \tilde{h}_{i\uparrow,j\sigma'}c_{j\sigma'} + \Delta_{ii}c^{\dagger}_{i\downarrow}, \\ [c^{\dagger}_{i\uparrow}, \mathscr{H}_{eff}] &= -\sum_{j\sigma'} \tilde{h}_{j\sigma',i\uparrow}c^{\dagger}_{j\sigma'} - \Delta^{*}_{ii}c_{i\downarrow}, \\ [c_{i\downarrow}, \mathscr{H}_{eff}] &= \sum_{j\sigma'} \tilde{h}_{i\downarrow,j\sigma'}c_{j\sigma'} - \Delta_{ii}c^{\dagger}_{i\downarrow}, \\ [c^{\dagger}_{i\downarrow}, \mathscr{H}_{eff}] &= -\sum_{j\sigma'} \tilde{h}_{j\sigma',i\downarrow}c^{\dagger}_{j\sigma'} + \Delta^{*}_{ii}c_{i\uparrow}.\end{aligned} \tag{21}$$

From this we can conclude that $c_{i\sigma}$ and $c^{\dagger}_{i\sigma}$ no longer are a good basis. In order to find a better basis we would like to express the electron field operators as linear combinations of electron- and hole-like quasiparticle excitations, which we do by performing the following Bogoliubov canonical transformation [22],

$$c_{i\sigma} = {\sum_{n}}'(u^{n}_{i\sigma}\gamma_n - \sigma v^{n*}_{i\sigma}\gamma^{\dagger}_n), \qquad c^{\dagger}_{i\sigma} = {\sum_{n}}'(u^{n*}_{i\sigma}\gamma^{\dagger} - \sigma v^{n}_{i\sigma}\gamma_n). \tag{22}$$

where $\sigma = \pm 1$ denote the up and down spin orientations and $\gamma^{\dagger}_n$ and γ_n are operators that create and annihilate a Bogoliubov quasiparticle at state n. These quasiparticles anticommute, i.e. $\{\gamma_n, \gamma_m\} = \{\gamma^{\dagger}_n, \gamma^{\dagger}_m\} = 0$ and $\{\gamma_n, \gamma^{\dagger}_m\} = \delta_{nm}$. The prime sign over the summation sign indicates that only positive energy states are counted. By applying this canonical transformation to the effective Hamiltonian, it is diagonalized as

$$H_{eff} = \sum_{n} E_n\gamma^{\dagger}_n\gamma_n + E'_{const}. \tag{23}$$

We then substitute Eq. (22) into Eq. (21), using the following commutation relations

$$\begin{aligned}[\gamma^{\dagger}_n, H_{eff}] &= -E_n\gamma^{\dagger}_n, \\ [\gamma_n, H_{eff}] &= E_n\gamma_n,\end{aligned} \tag{24}$$

and comparing the terms containing $\gamma_n^\dagger$ and γ_n, we obtain the BdG equations [22]:

$$\begin{aligned} E_n u_{i\uparrow}^n &= \sum_{j\sigma'} \tilde{h}_{i\uparrow,j\sigma'} u_{j\sigma'}^n + \sigma_{ii} v_{i\downarrow}^n, \\ E_n u_{i\downarrow}^n &= \sum_{j\sigma'} \tilde{h}_{i\downarrow,j\sigma'} + \Delta_{ii} v_{i\uparrow}^n, \\ E_n v_{i\uparrow}^n &= -\sum_{j\sigma'} \sigma' \tilde{h}_{i\uparrow,j\sigma'} v_{j\sigma'}^n + \Delta_{ii}^* u_{i\downarrow}^n, \\ E_n v_{i\downarrow}^n &= \sum_{j\sigma'} \sigma' \tilde{h}_{j\sigma',i\downarrow} v_{j\sigma'}^n + \Delta_{ii}^* u_{i\uparrow}^n, \end{aligned} \tag{25}$$

with the following self-consistency condition for the singlet-pairing potential:

$$\Delta_{ii} = \frac{U}{2} \sum_n{}' (u_{i\uparrow}^n v_{i\downarrow}^{n*} + u_{i\downarrow}^n v_{i\uparrow}^{n*}) \tanh\Big(\frac{E_n}{2k_B T}\Big). \tag{26}$$

It can be shown from the BdG equations in Eq. (25) that if $(u_{i\uparrow}^n, v_{i\downarrow}^n, u_{i\downarrow}^n, v_{i\uparrow}^n)$ solves the BdG equations for the eigenvalue E_n, it follows that $(-v_{i\uparrow}^{n*}, u_{i\downarrow}^{n*}, v_{i\downarrow}^{n*}, -u_{i\uparrow}^{n*})$ solves them for the eigenvalue $-E_n$. Using this, we can simplify the self-consistency condition to [22]

$$\Delta_{ii} = \frac{U}{2} \sum_n u_{i\uparrow}^n v_{i\downarrow}^{n*} \tanh\Big(\frac{E_n}{2k_B T}\Big). \tag{27}$$

Note that Δ_{ii} is the order parameter quantifying the superconductivity, meaning that Δ_{ii} will be zero above the critical temperature T_c. One way of solving the self-consistency is by making an initial guess for Δ_{ii} and using it to solve the BdG equations, then using the result to calculate a new Δ_{ii}. The new Δ_{ii} is used to once again calculate the BdG equations, and the procedure is repeated until the difference between the new Δ_{ii} and the previous one is "small enough". We will however solve the self-consistently in a slightly more intricate way using the Polyak method, which is explained in Section 4.2.

In the absence of spin-flip scattering and spin-orbit coupling, i.e. $\tilde{h}_{i\uparrow,j\downarrow} = \tilde{h}_{i\downarrow,j\uparrow} = 0$, the BdG equations can be split into two sets of equations,

$$\begin{aligned} E_{\tilde{n}1} u_{i\uparrow}^{\tilde{n}1} &= \sum_j \tilde{h}_{i\uparrow,j\uparrow} u_{j\uparrow}^{\tilde{n}1} + \Delta_{ii} v_{i\downarrow}^{\tilde{n}1}, \\ E_{\tilde{n}1} v_{i\downarrow}^{\tilde{n}1} &= -\sum_j \tilde{h}_{i\downarrow,j\downarrow}^* v_{j\downarrow}^{\tilde{n}1} + \Delta_{ii}^* u_{i\uparrow}^{\tilde{n}1} \end{aligned} \tag{28}$$

and

$$\begin{aligned} E_{\tilde{n}2} u_{i\downarrow}^{\tilde{n}2} &= \sum_j \tilde{h}_{i\downarrow,j\downarrow} u_{j\downarrow}^{\tilde{n}2} + \Delta_{ii} v_{i\uparrow}^{\tilde{n}2}, \\ E_{\tilde{n}2} v_{i\uparrow}^{\tilde{n}2} &= -\sum_j \tilde{h}_{i\uparrow,j\uparrow}^* v_{j\uparrow}^n + \Delta_{ii}^* u_{i\downarrow}^{\tilde{n}2}, \end{aligned} \tag{29}$$

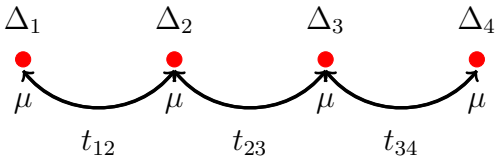

Figure 12: Tight-binding model of a 1D system with four sites. μ is the chemical potential, Δ_i are the pairing potentials and $t_{i,i+1}$ are the nearest neighbour hopping energies.

thus block-diagonalizing the BdG equation, reducing our matrix from $4N$ by $4N$ to $2N$ by $2N$, which improves the computational effiency significantly. With the symmetry between the solutions for the eigenvalues E_n and $-E_n$ and the block-diagonalization, it is enough to solve the first set of equations, in Eq. (28), with the following self-consistency condition

$$\Delta_{ii} = \frac{U}{2} \sum_{\tilde{n}} u_{i\uparrow}^{\tilde{n}1} v_{i\downarrow}^{\tilde{n}1*} \tanh\left(\frac{E_{\tilde{n}1}}{2k_B T}\right). \tag{30}$$

From here on, we drop the $\sim$ and the 1 in the subscript, as well as the second index i for Δ_{ii}.

The BdG equations in Eq. (28) can be written in a matrix form,

$$\sum_j \hat{M}_{ij} \hat{\phi}_j = E_n \hat{\phi}_i, \tag{31}$$

where

$$\hat{M}_{ij} = \begin{bmatrix} \tilde{h}_{i\uparrow,j\uparrow} & \Delta_{ij} \\ \Delta_{ji}^* & -\tilde{h}_{i\downarrow,j\downarrow}^* \end{bmatrix}, \qquad \hat{\phi}_i = \begin{bmatrix} u_{i\uparrow}^n \\ v_{i\downarrow}^n \end{bmatrix}. \tag{32}$$

For a 1D system, with only nearest neighbour hopping and without impurities, the matrix will look as follows,

$$H_{BdG}\phi = \begin{bmatrix} -\mu & t_{12} & 0 & 0 & \Delta_1 & 0 & 0 & 0 \\ t_{12} & -\mu & t_{23} & 0 & 0 & \Delta_2 & 0 & 0 \\ 0 & t_{23} & -\mu & t_{34} & 0 & 0 & \Delta_3 & 0 \\ 0 & 0 & t_{34} & -\mu & 0 & 0 & 0 & \Delta_4 \\ \Delta_1^* & 0 & 0 & 0 & \mu^* & -t_{12}^* & 0 & 0 \\ 0 & \Delta_2^* & 0 & 0 & -t_{12}^* & \mu^* & -t_{23}^* & 0 \\ 0 & 0 & \Delta_3^* & 0 & 0 & -t_{23}^* & \mu^* & -t_{34}^* \\ 0 & 0 & 0 & \Delta_4^* & 0 & 0 & -t_{34}^* & \mu^* \end{bmatrix} \begin{bmatrix} u_{1\uparrow} \\ u_{2\uparrow} \\ u_{3_\uparrow} \\ u_{4_\uparrow} \\ v_{1_\downarrow} \\ v_{2_\downarrow} \\ v_{3_\downarrow} \\ v_{4_\downarrow} \end{bmatrix} \tag{33}$$

where we have assumed the chemical potential, μ, to be the same at all sites. The same system can be seen in Fig. 12.

4.1.2 Charge density

Once one has solved the BdG equations and found the eigenvalues E_n and their corresponding eigenvectors, these can be used to calculate quantities such as the charge density and the density of states. The charge density is calculated as [22]

$$\begin{aligned} n_{i\uparrow} &= \sum_n |u^n_{i\uparrow}|^2 f(E_n), \\ n_{i\downarrow} &= \sum_n |v_{i\downarrow}|^2 f(-E_n), \end{aligned} \tag{34}$$

where $f(E) = 1/(\exp(E/k_BT) + 1)$ is the Fermi-Dirac distrubution and the total charge density is $n_i = n_{i\uparrow} + n_{i\downarrow}$.

4.1.3 Density of states

The density of states is the proportion of states that will be occupied at a certain energy E for a system. The local density of states at a site i can be calculated as [23]

$$\mathscr{N}_i(E) = -\frac{1}{\pi} \operatorname{Im} \sum_n \Big[\frac{|\langle u^n_i | u^n_i \rangle|^2}{E - E_n + i\eta} + \frac{|\langle v^n_i | v^n_i \rangle|^2}{E + E_n + i\eta} \Big], \tag{35}$$

where $\eta > 0$ is a small imaginary part of the energy. To get the total density of states one has to sum up the local density of states over all sites. The integrated density of states, idos(E), is calculated by integrating the normalized density of states up to the energy E,

$$\text{idos}(E) = \int_{-\infty}^{E} \mathscr{N}_T(E')dE', \tag{36}$$

where $\mathscr{N}_T$ is the normalized total density of states.

4.1.4 Bond current

An important observable for this project is the bond current, which can be derived from the Heisenberg equation of motion for the charge density $\langle n_i \rangle = \langle n_{i\uparrow} \rangle + \langle n_{i\downarrow} \rangle$ [22]:

$$\begin{aligned} i\hbar \frac{\partial \langle n_i \rangle}{\partial t} &= \langle [n_i, H]_- \rangle \\ &= \langle (- \sum_{j \neq i, \sigma, \sigma'} [-t_{j\sigma', i\sigma} c^\dagger_{j\sigma'} c_{i\sigma} + t_{i\sigma, j\sigma'} c^\dagger_{i\sigma} c_{j\sigma'}] \rangle, \end{aligned} \tag{37}$$

where H is the Hamiltonian in Eq. (15). The electrical current operator from site j to site i will then be

$$\hat{J}_{ij} = \frac{e}{i\hbar} \sum_{\sigma, \sigma'} [t_{i\sigma, j\sigma'} c^\dagger_{i\sigma} c_{j\sigma'} - t_{j\sigma', i\sigma} c^\dagger_{j\sigma'} c_{i\sigma}]. \tag{38}$$

The average bond current is then

$$J_{ij} = \frac{e}{i\hbar} \sum_{\sigma,\sigma'} \sum_{n}^{'} (t_{i\sigma,j\sigma'} [u_{i\sigma}^{n*} u_{j\sigma'}^{n} f(E_n) + \sigma\sigma' v_{i\sigma}^{n} v_{j\sigma'}^{n*} (1 - f(E_n)] - c.c.), \tag{39}$$

which can be rewritten using the symmetry properties of the BdG equations to

$$J_{ij} = \frac{4e}{i\hbar} \sum_{n} (t_{ij} u_i^{n*} u_j^n f(E_n) - t_{ij}^* u_j^{n*} u_i^n f(E_n)), \tag{40}$$

where we have also assumed that there are no spin-flip scattering or spin-orbit coupling.

4.2 Self-consistency: Convergence accelerator

The self-consistency in the order parameter, Δ_i, was solved by employing a convergence accelerator, namely the Polyak method [24]. The first few steps are the same as for a simple self-consistency procedure (where the calculated order parameter is naively put as the next guess). The convergence accelerator is then introduced when it is time to make a new guess, in Eq. (43). The algorithm begins by making an initial guess for Δ_i and using that to solve the BdG equations in Eq. (28). The solution is then used to calculate the order parameter again, in the following way

$$\Delta_i^{calc} = U \langle c_{i\downarrow} c_{i\uparrow} \rangle = U \sum_n u_{i\uparrow}^n v_{i\downarrow}^{n*} f(E_n). \tag{41}$$

Note that we did not use Eq. (30) for Δ_i, this is because that formulation is better suited for analytical work. The derivation of this expression can be found in Appendix A.1. We then check whether $max(|\Delta_i^{diff}|) < tol$, where tol is a set tolerance and

$$\Delta_i^{diff} = \Delta_i^{calc} - \Delta_i^{old}, \tag{42}$$

where Δ_i^{old} is the order parameter which was used to solve the system. If the largest difference in Δ_i is larger than the tolerance, we continue iterating, solving the BdG equations with a new guess for Δ_i. We do however not naively put in Δ_i^{calc} as our new guess, but use the Polyak method, as it converges a lot faster and is more stable:

$$\begin{aligned} v_i^{new} &= (1 - \beta) v_i^{old} + \alpha \Delta_i^{diff}, \\ \Delta_i^{new} &= \Delta_i^{old} + v_i^{new}, \end{aligned} \tag{43}$$

where $\beta \in (0, 1)$ is the drag and $\alpha > 0$ is the stepsize. v_i^{old} is initially set to be zero. Δ_i^{new} is the new guess for which we solve the BdG equations. This procedure is then repeated until $max(|\Delta_i^{diff}|)$ is smaller than the given tolerance. The method is also described step by step in Table 2.

Solving BdG self-consistently using the Polyak method
1. Make an initial guess for Δ_i. Set $v_i^{old} = 0$ and $\Delta_i^{old} = \Delta_i^{init}$.
2. Solve BdG equations in Eq. (28).
3. Calculate Δ_i^{calc} using Eq. (41).
4. Check tolerance, i.e. check if $max(\lvert\Delta_i^{diff}\rvert) < tol$.
If false go to step 5. If true go to step 6.
5. Calculate v_i^{new} and Δ_i^{new} according to Eq. (43).
Set $v_i^{old} = v_i^{new}$ and $\Delta_i^{old} = \Delta_i^{new}$ and go back to step 2.
6. Stop iterating and return final solution to the BdG equations.

Table 2: The BdG method was solved self-consistently in Δ_i using the Polyak method.

5 SNS-junctions

SNS-junctions and NS-junctions are hybrid systems that combine the effects of regions in the superconducting (S) and normal (N) state respectively. In the case of a nanowire, an NS-junction can for example be constructed by inducing superconductivity through proximity by placing part of the nanowire on a superconductor. If both ends of the nanowire are placed on superconductors, one will instead have an SNS-junction.

This section of the thesis discusses two phenomena found in SNS-junctions, the proximity effect and the Josephson current. First explaining the proximity effect, Section 5.1, and the Josephson current, Section 5.2, in regular, periodic SNS-junctions. Thereafter follows a discussion on quasicrystal SNS-junctions, where Section 5.3 details how the quasicrystal SNS-junction was modeled and Section 5.4 discusses the proximity effect in quasicrystals.

5.1 The proximity effect

When a system in the normal state is placed next to a superconducting system, the superconducting state will start to "spill" into the region in the normal state. This is referred to as the *proximity effect* [25]. This can be understood as a leakage of Cooper pairs from the superconducting region into the normal region. Even though there is no attractive electron-electron interaction in the normal region, i.e. $U = 0$, there can still be pair correlations. You may recall that the superconducting gap could be expressed as $\Delta_i = U\langle c_{i\downarrow}c_{i\uparrow}\rangle$, where U is by definition zero in the normal state, but where $F_i = \langle c_{i\downarrow}c_{i\uparrow}\rangle$ may be non-zero. The pair correlation can be expressed using the solution to the BdG equations as

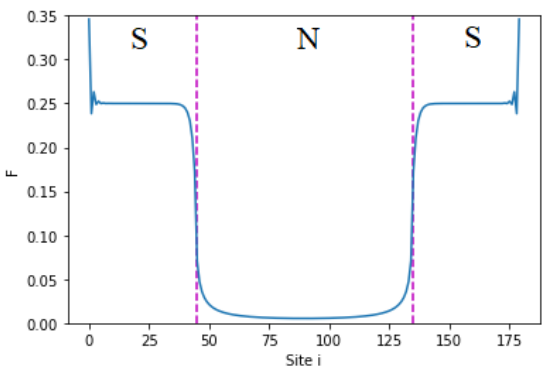

Figure 13: The proximity effect in an SNS-junction.

$$F_i = \sum_n u_{i\uparrow}^n v_{i\downarrow}^{n*} f(E_n), \tag{44}$$

where f is the Fermi-Dirac distribution. An example of the proximity effect in an SNS-junction can be seen in Fig. 13.

5.2 Andreev reflections and Josephson currents

An electron in a normal metal approaching an interface can either be reflected or transmitted according to scattering theory. However, if the region on the other side of the interface is superconducting another kind of reflection can occur, called *Andreev reflection* [26].

We begin by considering an electron in the normal part of an NS-junction, moving towards the interface, see Fig. 14. As the electron approaches the interface it may reflect or transmit normally, except that if the energy of the electron is smaller than the superconducting gap, $E < \Delta$, there are no available states in the superconducting part for the electron to transmit into. What instead can happen is that the electron is reflected as a hole, transferring a Cooper pair, which has charge $2e$, to the superconducting part.

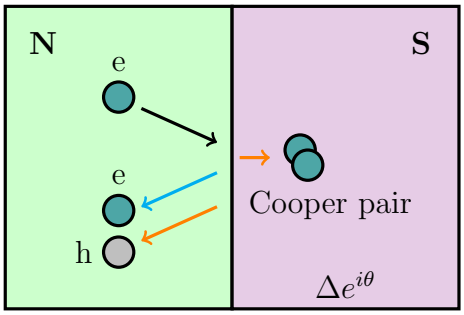

Figure 14: Andreev reflection in a NS-junction. A right-moving electron in the N part, $E < \Delta$, can be either normal reflected (cyan arrow) or Andreev reflected (orange arrow). If it is Andreev reflected, a Cooper pair is transferred to the S part.

We now consider an SNS-junction where the left superconductor has pairing potential $\Delta_L = \Delta e^{i\theta_L}$ and the right superconductor has pairing potential $\Delta_R = \Delta e^{i\theta_R}$, with a normal part of length L_N, see Fig. 15. A right-moving electron in the normal part, with energy $E < \Delta$, will be reflected as a hole at the right interface, leaving behind a Cooper pair in the right superconductor. The left-moving hole will then meet the left interface and reflect back as an electron, taking a Cooper pair from the left superconductor. As this cycle continues, Cooper pairs will be transferred from the left superconductor to the right superconductor, creating a *supercurrent* across the junction. Since the normal part has a finite length, L_N, discrete energy levels will form. If the phase difference, $\Delta\theta = \theta_R - \theta_L$, is non-zero, there will be standing bound waves with quantised energies in the SNS-junction. These states are known as *Andreev bound states* [27].

SNS-junctions can be divided into two different categories depending on the relation between the length of the normal part, L_N, and the superconducting coherence length [28], $\xi = \hbar v_F/\pi\Delta$, where $v_F = \hbar k_F/m$. *Short SNS-junctions* have normal parts that are much shorter than the coherence length, $L_N \ll \xi$, and *long SNS-junctions* have normal parts that are much longer than the coherence length, $L_N \gg \xi$.

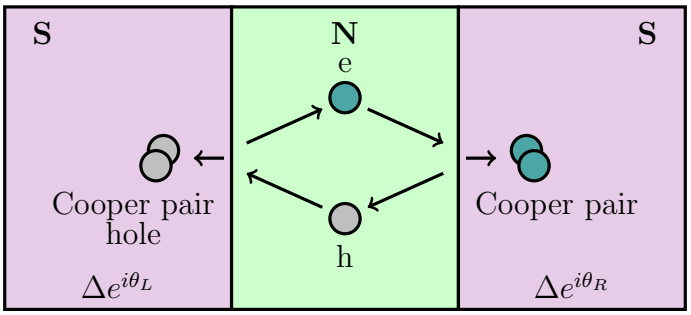

Figure 15: Schematic of an SNS junction. The electron reflects off the right interface as a hole, transmitting a charge $2e$ to the right superconductor. The hole will thereafter reflect off the left interface as an electron, taking a charge of $2e$ from the left superconductor. Through this process, Cooper pairs are transferred from the left to the right superconductor, creating a Josephson supercurrent.

As previously mentioned, the formation of Andreev bound states will also lead to the creation of a supercurrent flow across the junction. This will occur as long as there is a finite phase difference $\Delta\theta$ between the superconductors and is referred to as the *dc-Josephson effect*. The Josephson current can be calculated from the thermodynamic potential, F, as [25]

$$I(\Delta\theta) = \frac{2e}{\hbar}\frac{dF}{d(\Delta\theta)}, \tag{45}$$

where the factor 2 comes from the Cooper pair charge. This formula is general and applies to any type of Josephson junction. From the BdG equations, Eq. (45) can be written as [25], [29]

$$\begin{aligned} I(\Delta\theta) = &-\frac{2e}{\hbar}{\sum_n}' \tanh\left(\frac{E_n}{2\kappa_B T}\right)\frac{dE_n}{d(\Delta\theta)} \\ &-\frac{2e}{\hbar}2\kappa_B T\int_\Delta^\infty dE \ln\left[2\cosh\left(\frac{E}{e\kappa_B T}\right)\right]\frac{d\rho_c}{d(\Delta\theta)}, \end{aligned} \tag{46}$$

where $'$ denotes that we only sum over the positive eigenvalues. The first term contains the contributions from the discrete positive Andreev levels in the gap. The second term contains the contribution from excited states in the continuum above the gap where ρ_c is the density of states in the continuum.

For a short SNS-junction, the continuum density of states ρ_c is the same as in the bulk superconductor, and will therefore be phase independent [25]. This means that for short SNS-junctions and at $T = 0$, the Josephson current can be expressed as

$$I(\Delta\theta) = -\frac{2e}{\hbar}{\sum_n}' \frac{dE_n}{d(\Delta\theta)}. \tag{47}$$

5.3 Modeling SNS-junctions with quasicrystals

The system we study in this thesis is a nanowire following the modulation of a single Fibonacci approximant (not repeated), with two superconducting leads attached on either side of the quasiperiodic nanowire. This is compared to a regular SNS-junction, where the normal part between the superconducting leads is periodic. The system is modeled using the Hamiltonian in Eq. (15), where $U = 0$ in the normal part and $U = 2.5t_B$ in the superconducting parts. In the normal part the hopping energies are either t_A or t_B, according to the modulation of a given Fibonacci approximant. In the superconductors the hopping energies are set to $t_S = t_B$, and the hopping t_{int} between the superconductors and the normal parts are set to $t_{int} = t_B$ unless otherwise specified. The chemical potential is set to $\mu = 0$ everywhere. The setup is also illustrated in Fig. 16.

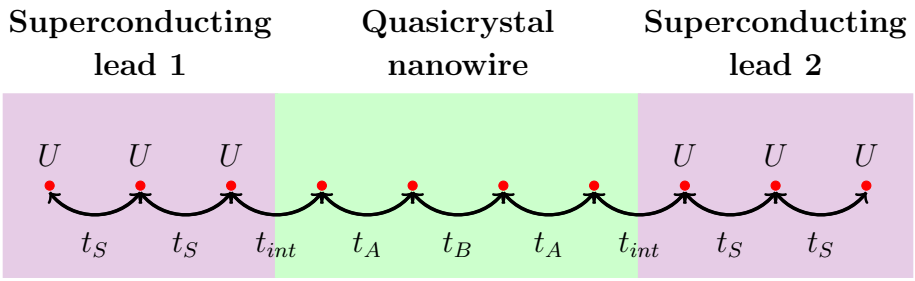

Figure 16: Tight-binding model of a 1D SNS-junction. The violet parts are superconducting leads attached to normal part in green.

5.4 The proximity effect in quasicrystals

In a regular, clean, and periodic SNS-junction, the proximity effect typically displays an exponential and smooth decay. This is however not the case as one replaces the periodic normal part with a Fibonacci quasicrystal, see Fig. 17. The pair correlation F in the normal part will then become heavily modulated, making it difficult to compare how long the proximity effect reaches in the quasicrystal compared to the periodic case. In order to be able to compare them, a curve fit is made to the pair correlation in the quasiperiodic normal part. Studies made on superconductor-quasicrystal hybrid rings [6], have found the best fit to the pair correlation in the quasiperiodic normal part to be

$$F_i^{fit} = a + b[i^{-c} + (L + 1 - i)^{-c}], \tag{48}$$

where L is the effective Fibonacci chain length. The best fit is found when including one site on each side of the proper Fibonacci chain, i.e. displacing the interface by one site on both sides of the Fibonacci chain, which means we have $L = N_{fib} + 2$, where N_{fib} is the length of the proper Fibonacci chain. i is the position, and since

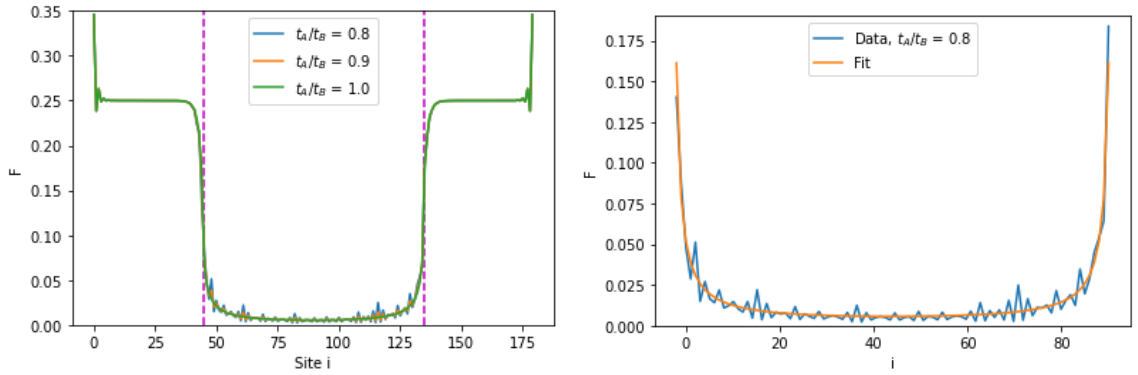

Figure 17: The pair correlation F for an SNS-junction with a 90 sites long quasicrystal, Fibonacci approximant $n = 10$ (left). The superconducting leads are 45 sites long and the superconducting phase difference is set to $\Delta\theta = 0$. The purple vertical lines show the positions of the interfaces between the superconducting and normal parts. A curve fit is made to the quasiperiodic normal part, of which an example is shown for $t_A/t_B = 0.8$ (right), with fitting parameters $a = 5.0429 \cdot 10^{-05}$, $b = 0.15980$ and $c = 1.0520$.

the decay is assumed to be symmetric, the leftmost position is set to $i = 1$ and the rightmost position is set to $i = L$. The parameters a, b, c are found by curve fitting using least squares. An example of a curve fit can be seen in Fig. 17.

One measure of the decay of the proximity effect in the quasicrystal could then be the decay length c. It was however found that c differ significantly depending on how the curve fit is done [6], e.g. if $L = N_{fib}$ instead of $L = N_{fib} + 2$. Instead, the value of the pair correlation in the middle of the curve fit, F_{mid}, is chosen as the measure of the proximity effect, since this remain closely the same for different choices of L.

6 Results for quasicrystal SNS-junctions

This section contains the results for the proximity effect, Section 6.1, and the Josephson current, Section 6.2, in a superconductor-quasicrystal-superconductor junction. For the proximity effect, the results in the quasicrystal SNS-junction should be comparable to that of a superconductor-quasicrystal hybrid ring [6], as long as the superconducting phase difference, $\Delta\theta$, is set to zero. For the proximity effect we only study the case of $\Delta\theta = 0$, since most of our focus is on the results for the Josephson current, as those are more novel and significant results. In order to be able to compare with the results for the superconductor-quasicrystal hybrid ring, we chose to look at two Fibonacci quasicrystals in particular, the 9:th approximant which is 56 sites long and the 10:th approximant which is 90 sites long. In all cases the superconducting leads are 45 sites long and the tolerance for the self-consistency is set to $tol = 10^{-5}$.

6.1 The proximity effect

The proximity effect is studied by taking the central value, F_{mid}, of the curve fit, described in Section 5.4. Figure 18 shows how F_{mid} changes as the phason angle ϕ is varied. Three different hopping ratios are plotted, the quasiperiodic $t_A/t_B = 0.8, 0.9$, as well as the periodic case $t_A/t_B = 1$. The periodic case remains constant as ϕ is varied, since phason flips can not occur in a periodic structure. For $t_A/t_B = 1$, F_{mid} is taken as the value of the pair correlation F in the middle of the chain, and not by doing a curve fit. The superconducting phase difference is set to $\Delta\theta = 0$.

One may note that for some phason angles F_{mid} is larger in the quasiperiodic chain than in the periodic chain. The difference is however quite small, and thus we have plotted the pair correlation F and the corresponding curve fit for the the maximal and minimal F_{mid} in Fig. 19 for $n = 9$ and in Fig. 20 for $n = 10$.

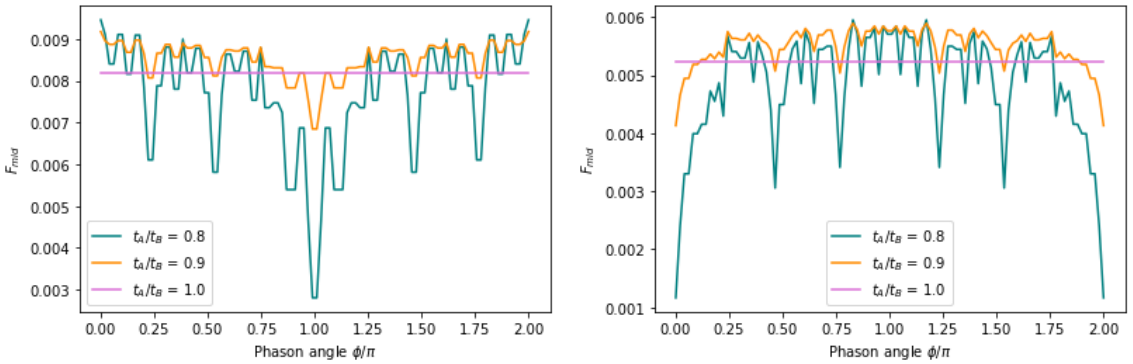

Figure 18: F_{mid} plotted as a function of the phason angle ϕ for two different Fibonacci approximants, $n = 9$ (left), which is 56 sites long, and $n = 10$ (right), which is 90 sites long. The superconducting phase difference is $\Delta\theta = 0$.

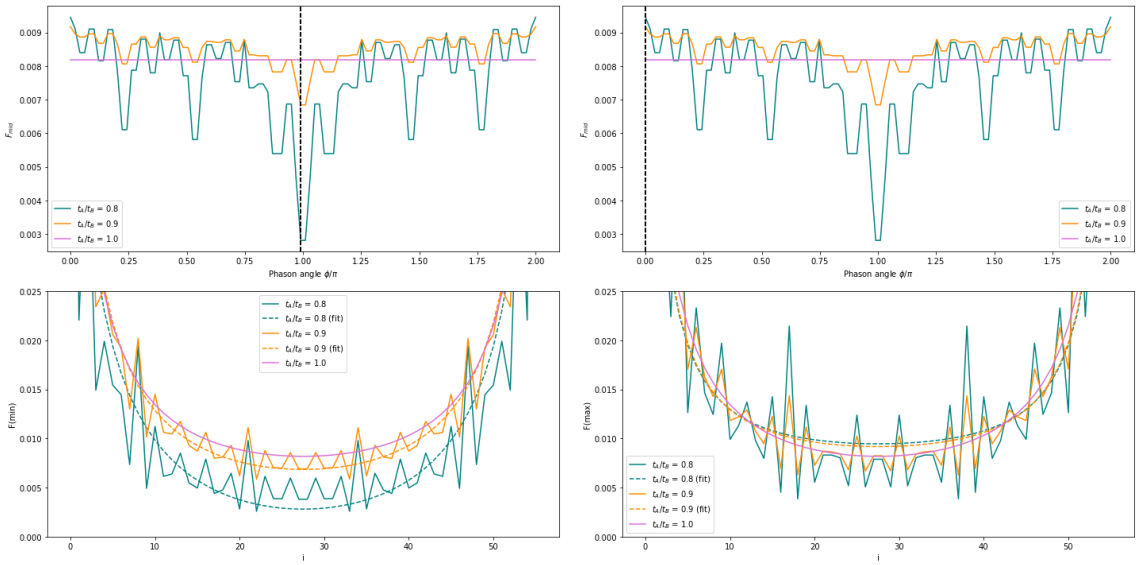

Figure 19: The minimal and maximal F_{mid} for Fibonacci approximant $n = 9$. The upper plots display the chosen phason angle for the minimal and maximal values of F_{mid} respectively. The lower plots show the corresponding pair correlation F and curve fit as a function of position, with the minimal F_{mid} to the left and the maximal F_{mid} to the right.

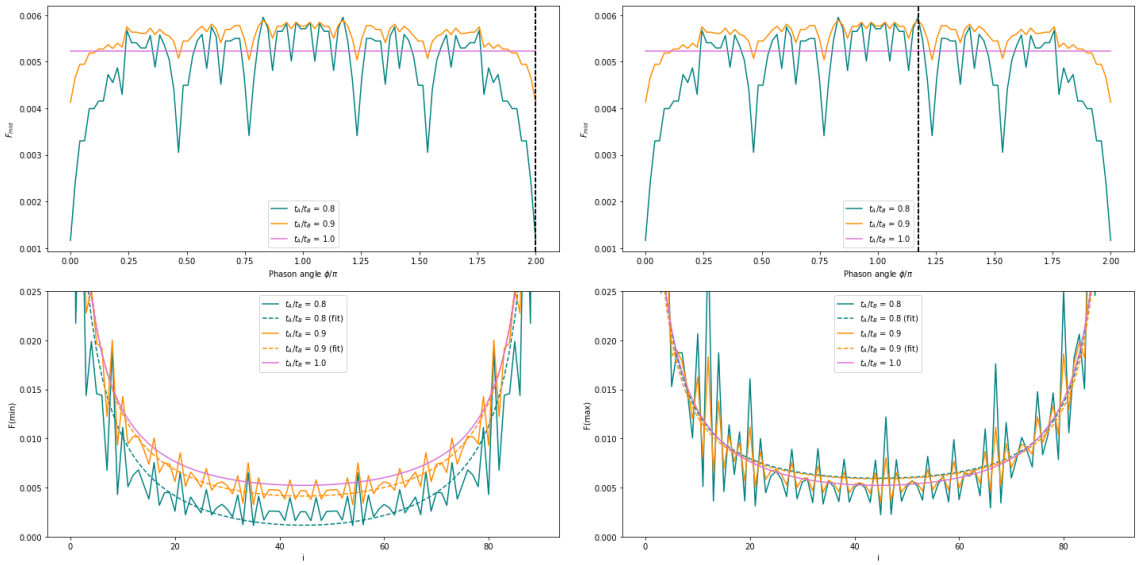

Figure 20: The same plots as in Fig. 19, but for Fibonacci approximant $n = 10$.

6.2 Josephson currents

This section presents the results for the Josephson current, first as a function of the superconducting phase difference, $\Delta\theta$, and thereafter as a function of the phason angle,ϕ, and the interface hopping, t_{int}, respectively. The current over the junction is calculated using Eq. (40), an example of which is shown in Fig. 21. The Josephson current as a function of the superconducting phase difference $\Delta\theta$ is shown in Fig. 22 for the hopping ratios $t_A/t_B = 0.8, 0.9, 1$. For certain values of the superconducting phase difference, around $\Delta\theta = \pi$, the quasiperiodic chains carry a larger current than the periodic chain. For $n = 9$, the current is only larger for $t_A/t_B = 0.9$, but for $n = 10$, both $t_A/t_B = 0.8$ and $t_A/t_B = 0.9$ carry larger currents than the periodic chain for certain phase differences.

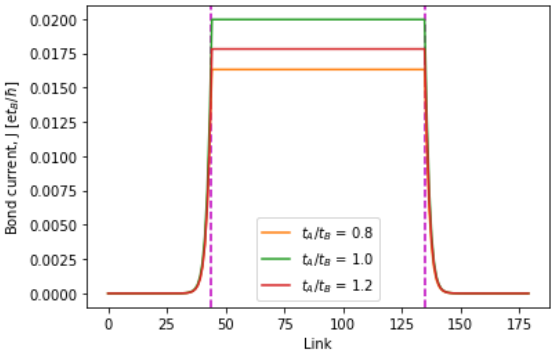

Figure 21: The bond current as function of position (link) for Fibonacci approximant $n = 10$. The superconducting phase difference is set to $\Delta\theta = -\pi/2$. The purple dashed lines mark the location of the interfaces. The phason angle is set to $\varphi = \phi_0$ ($\phi = \phi_0 + c_n$). The interface hopping is set to $t_{int} = t_B$.

Figure 23 shows the Josephson current as a function of the phason angle ϕ, also for the hopping ratios $t_A/t_B = 0.8, 0.9, 1$, for the fixed superconducting phase difference $\Delta\theta = 1.1\pi$. All other figures display chains where the phason angle is set to $\varphi = \phi_0$.

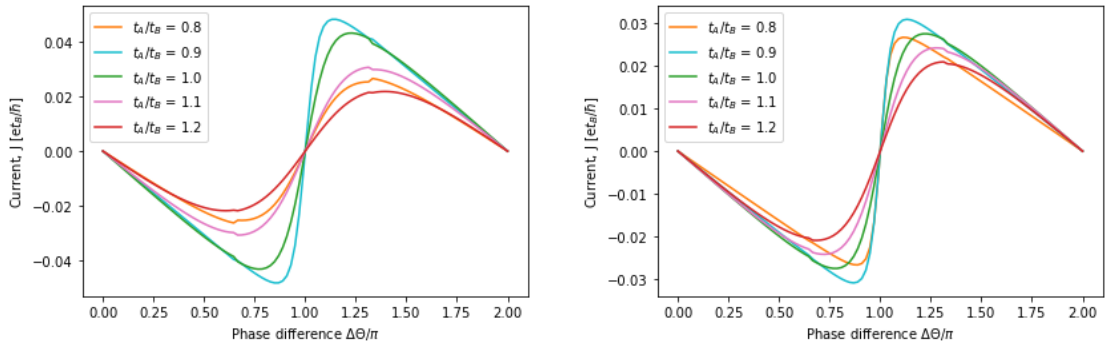

Figure 22: The Josephson current as a function of the superconducting phase difference for Fibonacci approximants $n = 9$ (left) and $n = 10$ (right). The phason angle is set to $\varphi = \phi_0$ and the interface hopping is $t_{int} = t_B$.

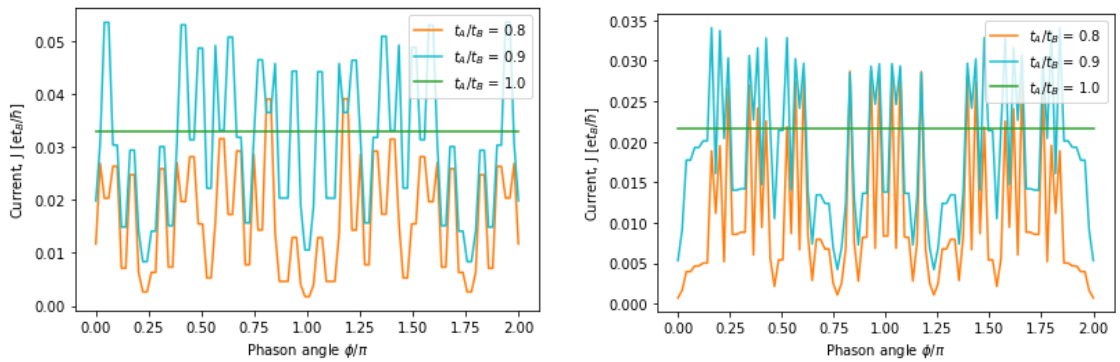

Figure 23: The Josephson current as a function of the phason angle for Fibonacci approximants $n = 9$ (left) and $n = 10$ (right). The superconducting phase difference is set to $\Delta\theta = 1.1\pi$ and the interface hopping is set to $t_{int} = t_B$.

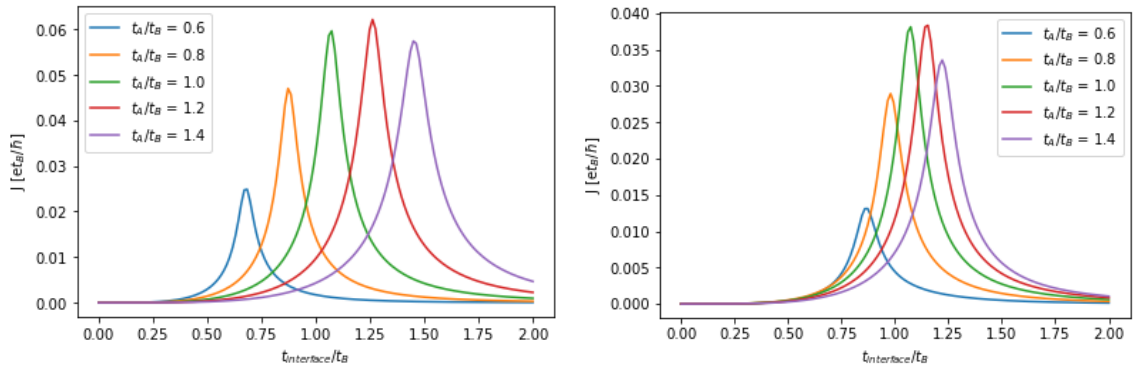

Figure 24: The Josephson current as a function of the interface hopping t_{int} for Fibonacci approximants $n = 9$ (left) and $n = 10$ (right). The superconducting phase difference is set to $\Delta\theta = 1.1\pi$ and the phason angle is $\varphi = \phi_0$.

The periodic chain is as familiar not impacted by varying the phason angle, thus the current over the periodic junction remains constant as ϕ is varied. For certain ϕ values, the currents over the quasiperiodic junctions are larger than in the periodic one.

Figure 24 displays the current over the junction as a function of the interface hopping t_{int}, for the hopping ratios $t_A/t_B = 0.6, 0.8, 1, 1.2, 1.4$. The superconducting phase difference is set to $\Delta\theta = 1.1\pi$. Here it is interesting to note that the current peaks for different values of t_{int} depending on what value t_A/t_B is set to. For smaller ratios t_A/t_B the Josephson current peaks for a lower interface hopping t_{int}, and as t_A/t_B is increased the peak is shifted to higher values of t_{int}. For some of the quasiperiodic junctions, the current at the peak is an order of magnitude larger than in a periodic junction with the same value of t_{int}.

For the periodic case, the current peaks as the transparency over the interface is the largest, which occurs for interface hopping $t_{int} \approx t_B$. This is because the the electrons and holes then solely Andreev reflect, maximizing the Josephson current. As the interface hopping is decreased, the electrons and holes start to reflect "normally" more, and Andreev reflect less, leading to a decrease in current over the junction. We do not expect for the coupling between the superconducting and normal parts to be larger than the hoppings in the two parts respectively, this might be why the current decreases as the interface hopping increases past the peak.

One hypothesis for why the current peaks for a different interface hopping, t_{int}, in the quasiperiodic junctions than in the periodic one, has to do with backscattering. Because of the modulations in the quasiperiodic chain, as the electron (hole) Andreev reflect against the interface, there is a finite possibility that it then backscatters, and thereafter Andreev reflects again, forming a bound state. These bound states near the edges then makes it easier for the Cooper pairs to tunnel through the junction. Depending on the modulation and the hopping ratio, t_A/t_B, of the chain, these bound states would then occur for different values of t_{int}.

Figure 25 displays the Josephson current as a function of the phason angle for the 9:th Fibonacci approximant, with interface hopping $t_{int} = 0.88t_B$. The current over the junction is significantly larger in the quasicrystals for many values of the phason angle, often 4-5 times larger than the current in the periodic chain.

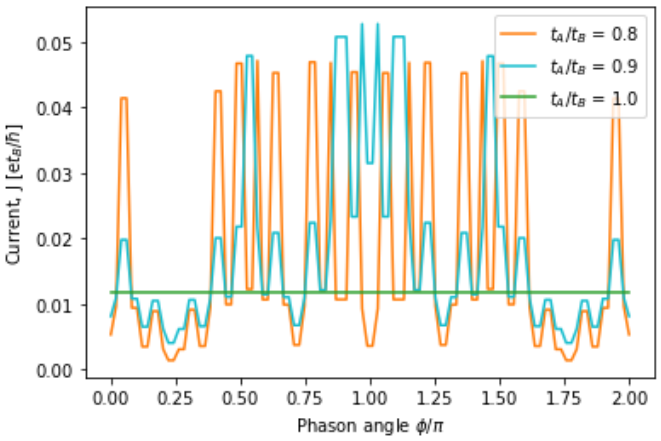

Figure 25: The current as a function of the phason angle for Fibonacci approximant $n = 9$, with interface hopping $t_{int} = 0.88t_B$. The superconducting phase difference $\Delta\theta = 1.1\pi$.

In order to understand the mechanisms behind the enhanced Josephson current, we start by studying the energy spectra. For short junctions it is mainly the positive eigenvalues within the superconducting gap that contribute to the Josephson current. Figures 26, 27 and 28 show the Josephson current and the positive energy eigenvalues within the superconducting gap, i.e. for $E < \Delta$, in the 9:th Fibonacci approximant, as a function of the superconducting phase difference $\Delta\theta$, for interface hoppings $t_{int} = 1.08, 0.88$ and 0.68 respectively. For each of the different figures, a different hopping ratio t_A/t_B displays the largest current. For $t_{int} = 1.08$ (Fig. 26), the periodic chain carries the largest current, for $t_{int} = 0.88$ (Fig. 27), the quasiperiodic

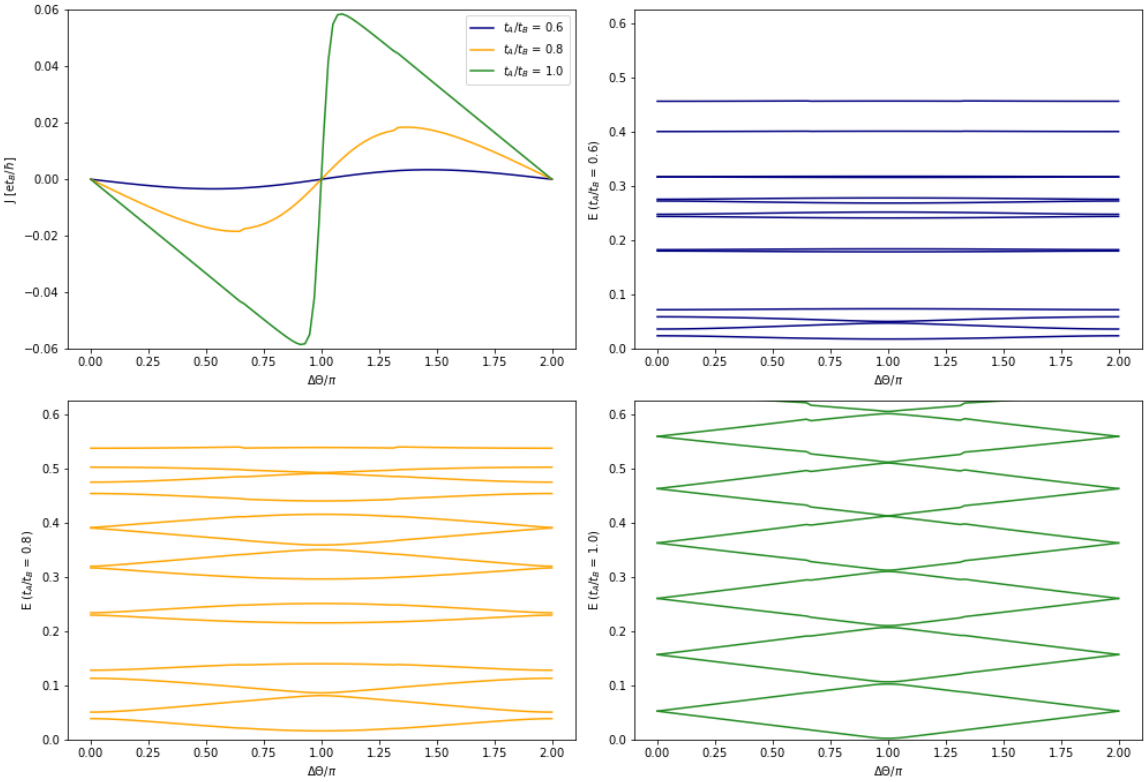

Figure 26: The upper left plot shows the Josephson current for Fibonacci approximant $n = 9$, as a function of the superconducting phase difference $\Delta\theta$, for the interface hopping $t_{int} = 1.08$. The remaining plots show the corresponding energy levels within the superconducting gap, Δ.

chain with hopping ratio $t_A/t_B = 0.8$ carries the largest current, and for $t_{int} = 0.68$ (Fig. 28), the quasiperiodic chain with hopping ratio $t_A/t_B = 0.6$ carries the largest current.

A way of analyzing the physics behind the Josephson current in quasicrystal junctions is by looking at the analytical expression for the Josephson current in Eq. (46) and comparing with the energy spectra, to see what part of the spectra contributes the most to the current. In short SNS-junctions it is primarily the positive Andreev levels in the gap that contribute to the Josephson current, as can be seen in Eq. (47). The current then depends on the sum of the slope of the positive energy levels in the gap, as a function of the superconducting phase difference, $\Delta\theta$. We do however not know whether our junctions fall in the short junction regime and it is difficult to qualitatively gather from the energy spectra in Fig. 26, 27 and 28 if the slope of the energy levels seem to account for the difference in the currents. A more conclusive way of determining whether the positive Andreev levels account for the Josephson current would be to calculate the Josephson current for a short junction using Eq. (47) and

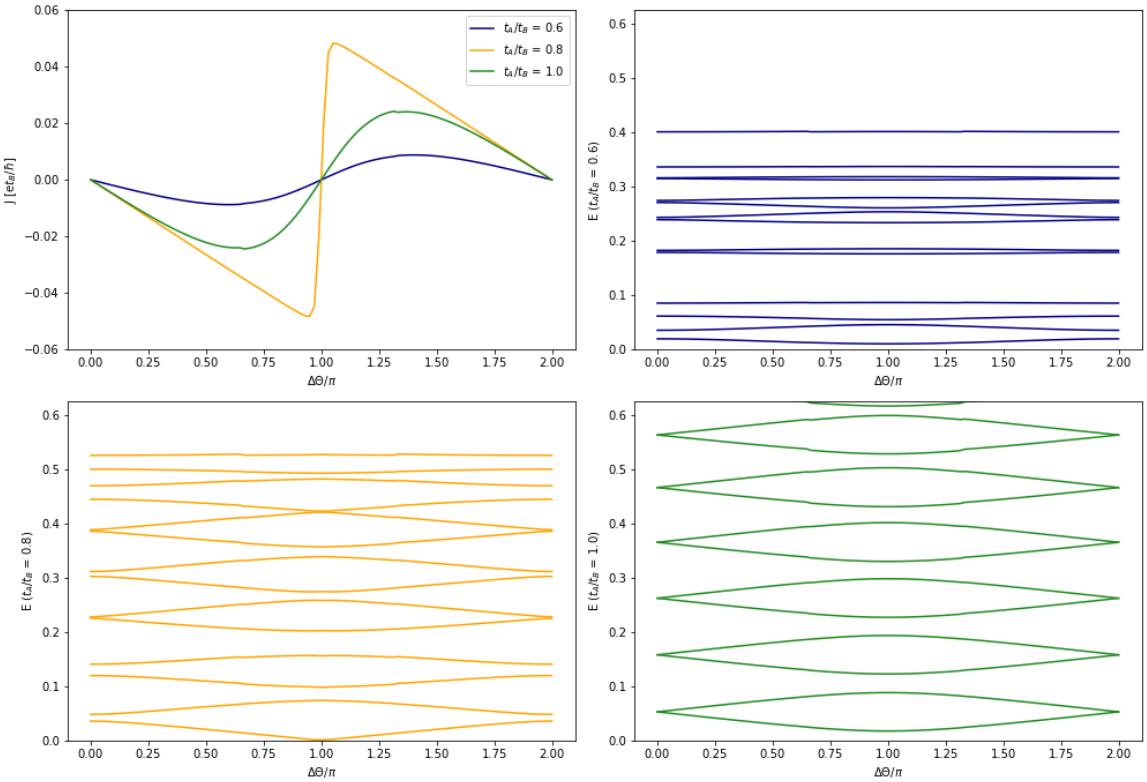

Figure 27: The upper left plot shows the Josephson current for Fibonacci approximant $n = 9$, as a function of the superconducting phase difference $\Delta\theta$, for the interface hopping $t_{int} = 0.88$. The remaining plots show the corresponding energy levels within the superconducting gap, Δ.

then compare it to the numeric results. Another way of understanding the physics behind the Josephson current in quasicrystals would be to study the edge modes, as they might enable Cooper pairs to tunnel more easily over the junction.

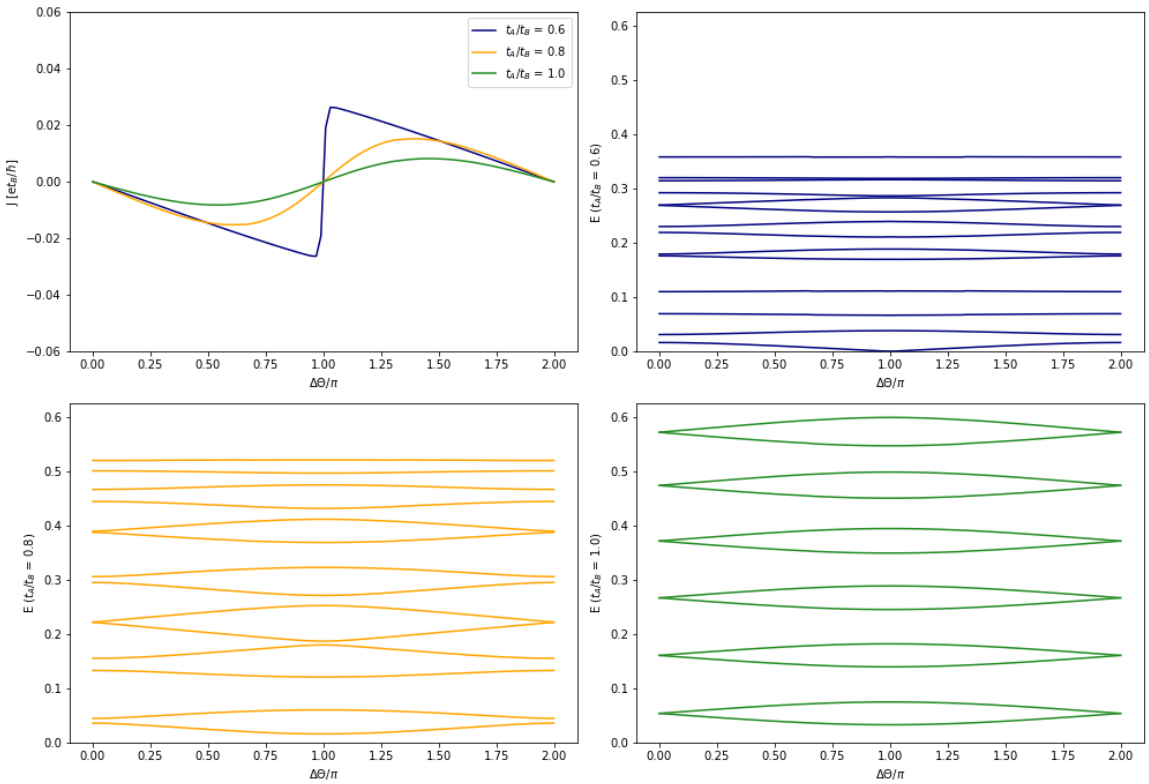

Figure 28: The upper left plot shows the Josephson current for Fibonacci approximant $n = 9$, as a function of the superconducting phase difference $\Delta\theta$, for the interface hopping $t_{int} = 0.68$. The remaining plots show the corresponding energy levels within the superconducting gap, Δ.

7 Conclusions and outlook

We have studied the proximity effect and the Josephson current in quasicrystal SNS-junctions by solving the Bogoliubov-de Gennes equations self-consistently. We found that the proximity effect could be somewhat enhanced by quasiperiodicity, as the value of F_{mid} was larger for some phason angles than in the periodic chain. Even though the relative difference was quite large, the absolute difference between the maximal F_{mid} in the quasiperiodic chains and the F_{mid} value in the periodic chain was rather small. This can also be seen in Fig. 19 and Fig. 20. As the pair correlation oscillates in the quasiperiodic chains it often takes on values that are lower than the periodic value of F, with some peaks that are significantly larger than the periodic pair correlation. Here we looked only at two different Fibonacci approximants, $n = 9$ and $n = 10$, so it could be that for some other quasicrystal chain the difference is more prominent.

The most interesting result of this thesis is that the Josephson current was found to be significantly larger in the quasiperiodic junctions than in the periodic junctions, for certain parameter choices. Figure 23 shows that the choice of phason angle strongly impacts the current over a quasiperiodic junction. The interface hopping t_{int} can have an even larger effect on the Josephson current, as can be seen in Fig. 24. Depending on the hopping ratio t_A/t_B, the current will peak for a different value of t_{int}. Lower hopping ratios t_A/t_B will peak for lower interface hopping t_{int} and vice versa, higher hopping ratios will peak for higher interface hoppings. At some of the peaks, the current in the quasiperiodic chains are one order of magnitude larger than in a periodic chain with the same interface hopping.

Thus far we have not been able to come with a conclusive answer as to what mechanisms lie behind the increased Josephson current in the quasicrystal SNS-junctions. To do so, it will be crucial to try to understand the energy spectra. One hypothesis for the enhanced current in the quasiperiodic chains is that the modulations in the chain give rise to bound states at the edges, enabling Cooper pairs to more easily tunnel through the normal part. Another one is that it is the critical states that facilitate the tunneling over the junction. This could be investigated by first looking at the probability density and the spectrum at the edges, as well as calculating the transparency or transmission at the interfaces.

Other possible outlooks for the 1D quasicrystal SNS-junction could be to investigate the effects of varying the chemical potential, μ, of the junction as a whole, or parts of it, as we have only studied the case of $\mu = 0$ for the whole system. Another interesting, but challenging, research question is to study if one can find a connection between the Josephson current and the topological properties of the quasicrystals. Furthermore, it would be of interest to extend this study to 2D quasicrystals to see if they also display significant enhancements in the Josephson current.

8 Acknowledgements

A research project is never done alone, and this master thesis would certainly not have been possible without the support of the people around me. I would first like to thank my supervisor Patric Holmvall for his support and guidance during this project, helping me navigate the physics of quasicrystals and superconductivity, and pitching in when I met obstacles in my code implementation. Without his counsel and encouragement this project would not have been possible. I would also like to extend my deepest gratitude to Annica Black-Schaffer for welcoming me into the research group and to my colleagues for their advice and support. A special thanks goes out to Rodrigo Arouca de Albuquerque, Tomas Löthman and Lucas Baldo Mesa Casa for answering any and every question. I would also like to thank Oladunyoje Awoga for his helpful advice. Last, but absolutely not least, I thank my friends and family for their support and encouragement. An extra thanks to my friend Tomas André for helping me with the programming and listening to me whine.

A Appendix

A.1 Pair correlation

The pair correlation F can be written in terms of the eigenvectors one gets from solving the Bogoliubov-de Gennes equations. We begin from the pair correlation

$$F = \langle c_{i\downarrow} c_{i\uparrow} \rangle, \tag{49}$$

plugging in the Bogoliubov transformation in Eq. (22),

$$\begin{aligned} \langle c_{i\downarrow} c_{i\uparrow} \rangle &= \sum_{n}{}' \langle (u^n_{i\downarrow} \gamma_n + v^{n*}_{i\downarrow} \gamma^\dagger_n)(u^n_{i\uparrow} \gamma_n - v^{n*}_{i\uparrow} \gamma^\dagger_n) \rangle \\ &= \sum_{n}{}' (u^n_{i\downarrow} u^n_{i\uparrow} \langle \gamma_n \gamma_n \rangle - u^n_{i\downarrow} v^{n*}_{i\uparrow} \langle \gamma_n \gamma^\dagger_n \rangle + u^n_{i\uparrow} v^{n*}_{i\downarrow} \langle \gamma^\dagger_n \gamma_n \rangle - v^{n*}_{i\downarrow} v^{n*}_{i\uparrow} \langle \gamma^\dagger_n \gamma^\dagger_n \rangle), \end{aligned} \tag{50}$$

where $'$ denotes that we only sum over positive eigenvalues. Using the following relations, $\langle \gamma_n \gamma_n \rangle = \langle \gamma^\dagger_n \gamma^\dagger_n \rangle = 0$, $\langle \gamma^\dagger_n \gamma_n \rangle = f(E_n)$ and $\langle \gamma_n \gamma^\dagger_n \rangle = 1 - \langle \gamma^\dagger_n \gamma_n \rangle$, we can rewrite the expression as

$$\begin{aligned} \langle c_{i\downarrow} c_{i\uparrow} \rangle &= \sum_{n}{}' (-u^n_{i\downarrow} v^{n*}_{i\uparrow} (1 - \langle \gamma^\dagger_n \gamma_n \rangle) + u^n_{i\uparrow} v^{n*}_{i\downarrow} \langle \gamma^\dagger_n \gamma_n \rangle) \\ &= \sum_{n}{}' (-u^n_{i\downarrow} v^{n*}_{i\uparrow} f(-E_n) + u^n_{i\uparrow} v^{n*}_{i\downarrow} f(E_n)), \end{aligned} \tag{51}$$

where $f(E_n) = 1/(\exp(E_n/k_B T) + 1)$ and $f(-E_n) = 1 - f(E_n)$.

Using the symmetry properties of the BdG equations, that if $(u^n_{i\uparrow}, v^n_{i\downarrow}, u^n_{i\downarrow}, v^n_{i\uparrow})$ solves the BdG equations for the eigenvalue E_n, it follows that $(-v^{n*}_{i\uparrow}, u^{n*}_{i\downarrow}, v^{n*}_{i\downarrow}, -u^{n*}_{i\uparrow})$ solves them for the eigenvalue $-E_n$, we end up with the final expression

$$F = \langle c_{i\downarrow} c_{i\uparrow} \rangle = \sum_{n} u^n_{i\uparrow} v^{n*}_{i\downarrow} f(E_n). \tag{52}$$

A.2 Results: Density of states for quasicrystal SNS-junctions

This appendix shows the results for the density of states for quasicrystal SNS-junctions, with Fibonacci approximant $n = 9$, for different interface hoppings, t_{int}.

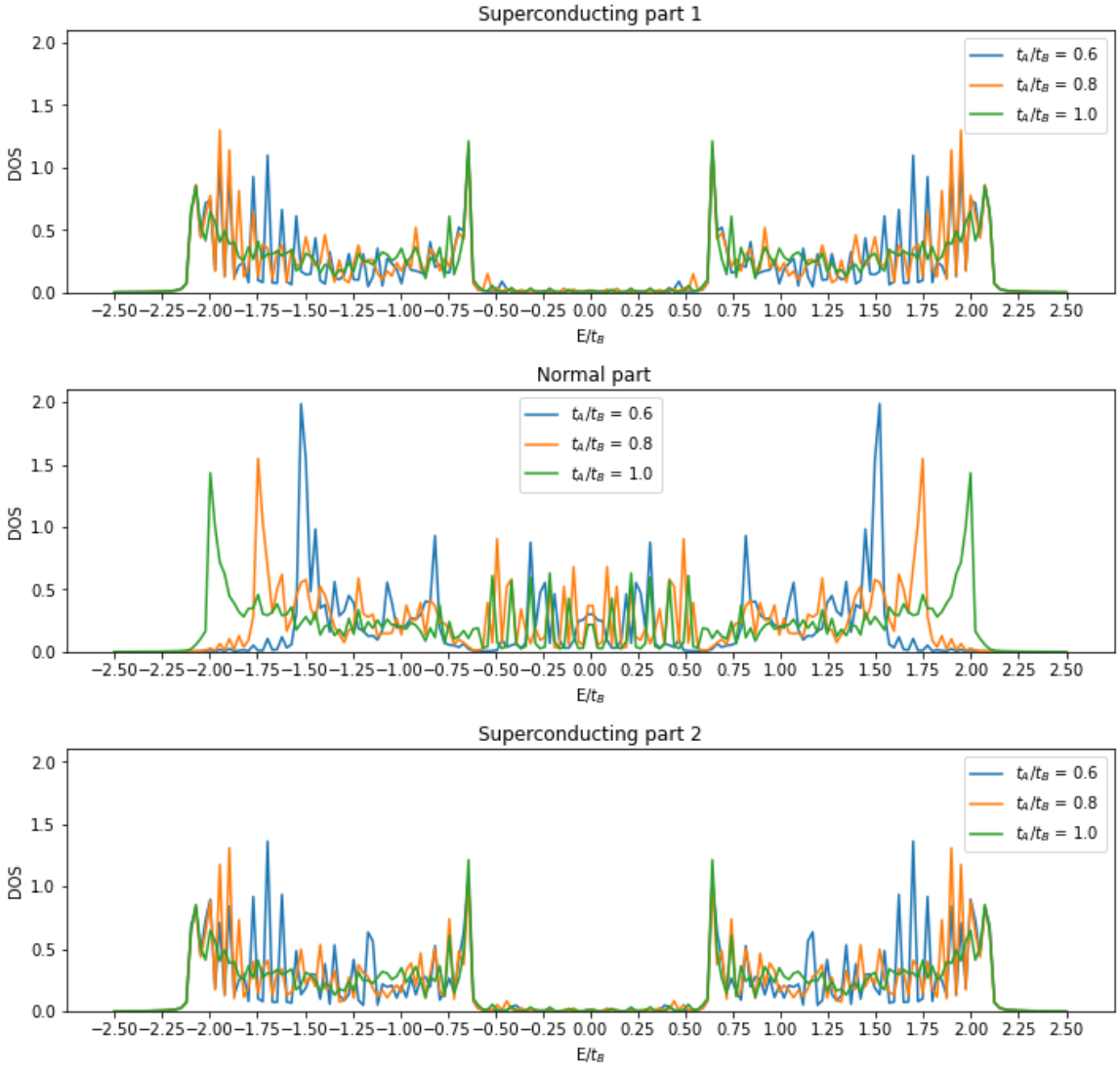

Figure 29: Density of states for an SNS-junction with Fibonacci approximant, $n = 9$. Interface hopping is set to $t_{int} = 1.08t_B$ and superconducting phase difference $\Delta\theta = 1.1\pi$.

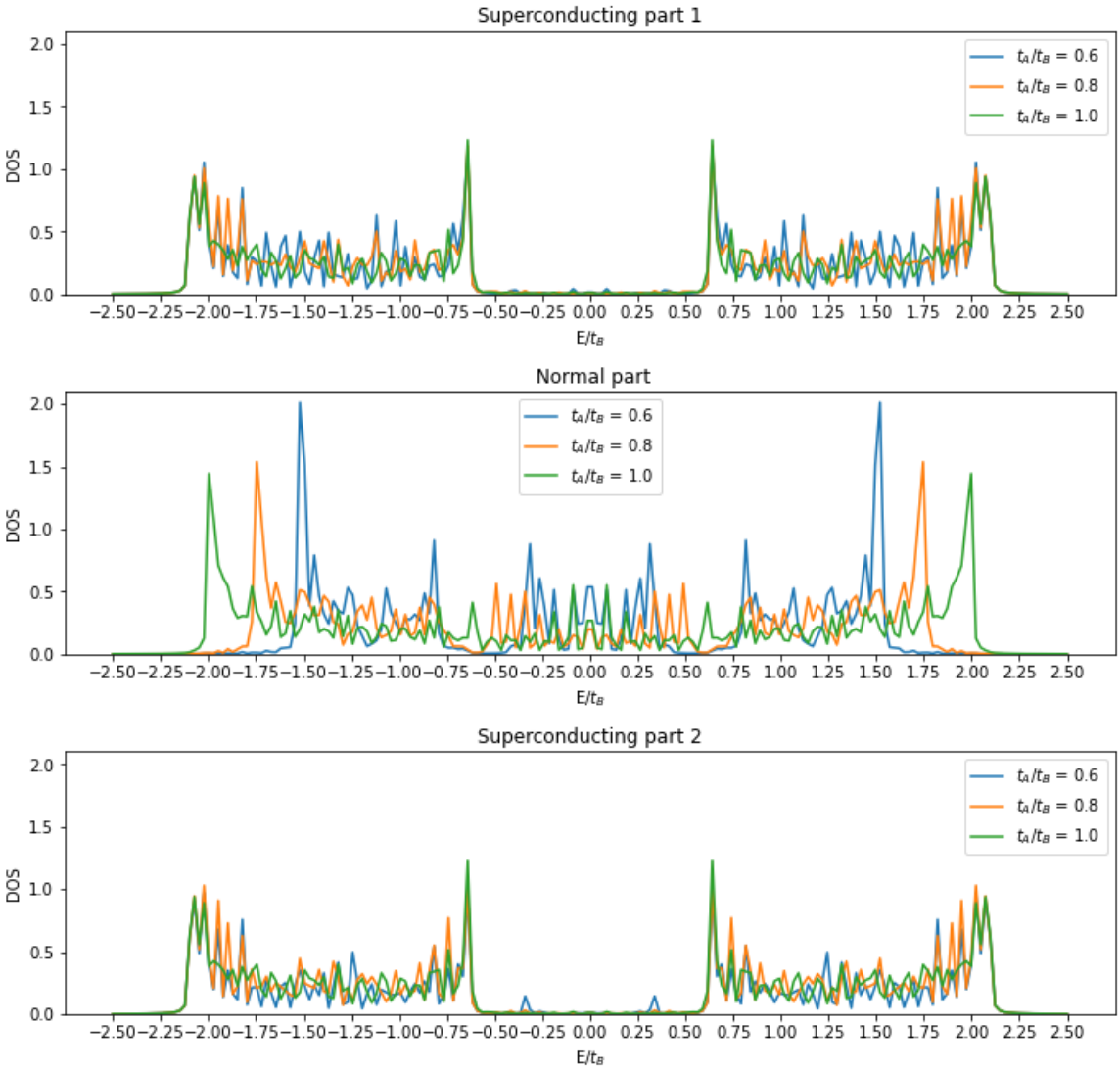

Figure 30: Density of states for an SNS-junction with Fibonacci approximant, $n = 9$. Interface hopping is set to $t_{int} = 0.88t_B$ and superconducting phase difference $\Delta\theta = 1.1\pi$.

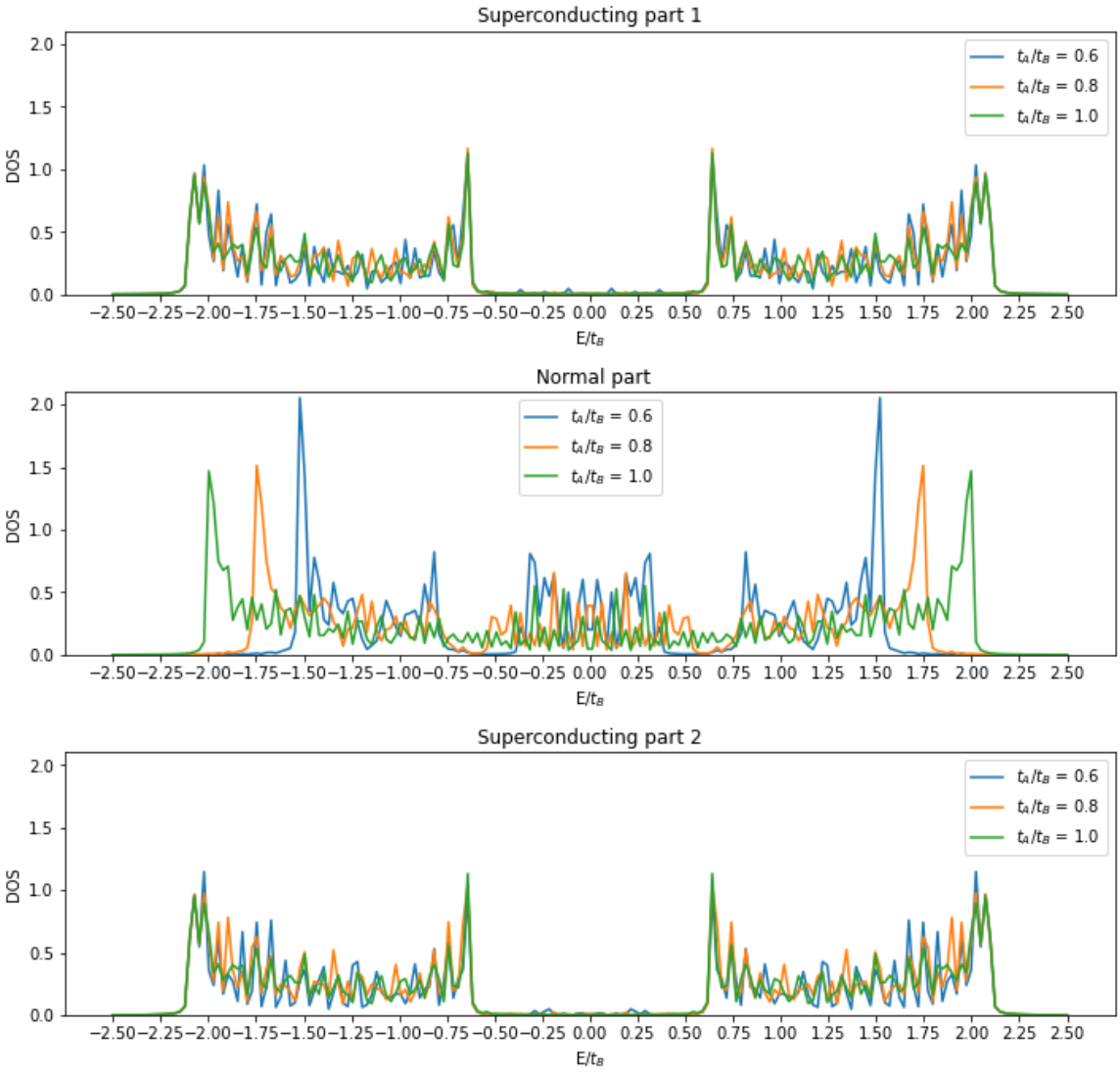

Figure 31: Density of states for an SNS-junction with Fibonacci approximant, $n = 9$. Interface hopping is set to $t_{int} = 0.68t_B$ and superconducting phase difference $\Delta\theta = 1.1\pi$.

References

[1] M. Gardner, "Mathematical Games", *Scientific American*, vol. 236, no. 1, 1977, ISSN: 0036-8733. DOI: 10.1038/scientificamerican0177-110.

[2] A. L. Mackay, "Crystallography and the penrose pattern", *Physica A: Statistical Mechanics and its Applications*, vol. 114, no. 1-3, pp. 609–613, Aug. 1982, ISSN: 03784371. DOI: 10.1016/0378-4371(82)90359-4.

[3] D. Shechtman, I. Blech, D. Gratias, and J. W. Cahn, "Metallic Phase with Long-Range Orientational Order and No Translational Symmetry", *Physical Review Letters*, vol. 53, no. 20, pp. 1951–1953, Nov. 1984, ISSN: 0031-9007. DOI: 10.1103/PhysRevLett.53.1951.

[4] L. C. Collins, T. G. Witte, R. Silverman, D. B. Green, and K. K. Gomes, "Imaging quasiperiodic electronic states in a synthetic Penrose tiling", *Nature Communications*, vol. 8, 2017, ISSN: 20411723. DOI: 10.1038/ncomms15961.

[5] K. Kamiya, T. Takeuchi, N. Kabeya, *et al.*, "Discovery of superconductivity in quasicrystal", *Nature Communications*, vol. 9, no. 1, 2018, ISSN: 20411723. DOI: 10.1038/s41467-017-02667-x.

[6] G. Rai, S. Haas, and A. Jagannathan, "Proximity effect in a superconductor-quasicrystal hybrid ring", *Physical Review B*, vol. 100, no. 16, p. 165 121, Oct. 2019, ISSN: 2469-9950. DOI: 10.1103/PhysRevB.100.165121.

[7] A. Jagannathan, "The Fibonacci quasicrystal: Case study of hidden dimensions and multifractality", *Reviews of Modern Physics*, vol. 93, no. 4, 2021, ISSN: 15390756. DOI: 10.1103/RevModPhys.93.045001.

[8] Y. E. Kraus and O. Zilberberg, "Topological equivalence between the fibonacci quasicrystal and the harper model", *Physical Review Letters*, vol. 109, no. 11, 2012, ISSN: 00319007. DOI: 10.1103/PhysRevLett.109.116404.

[9] J. Ledieu, J. T. Hoeft, D. E. Reid, *et al.*, "Pseudomorphic growth of a single element quasiperiodic ultrathin film on a quasicrystal substrate", *Physical Review Letters*, vol. 92, no. 13, 2004, ISSN: 00319007. DOI: 10.1103/PhysRevLett.92.135507.

[10] J. Bellissard, "Gap Labelling Theorems for Schrodinger Operators", in *From Number Theory to Physics*, Springer, 1992, pp. 538–630, ISBN: 978-3-642-08097-5. DOI: 10.1007/978-3-662-02838-4.

[11] N. Macé, A. Jagannathan, and F. Piéchon, "Gap structure of 1D cut and project Hamiltonians", in *Journal of Physics: Conference Series*, vol. 809, 2017. DOI: 10.1088/1742-6596/809/1/012023.

[12] Y. E. Kraus, Y. Lahini, Z. Ringel, M. Verbin, and O. Zilberberg, "Topological states and adiabatic pumping in quasicrystals", *Physical Review Letters*, vol. 109, no. 10, 2012, ISSN: 00319007. DOI: 10.1103/PhysRevLett.109.106402.

[13] D. Tanese, E. Gurevich, F. Baboux, *et al.*, "Fractal energy spectrum of a polariton gas in a fibonacci quasiperiodic potential", *Physical Review Letters*, vol. 112, no. 14, 2014, ISSN: 10797114. DOI: 10.1103/PhysRevLett.112.146404.

[14] F. Baboux, E. Levy, A. Lemaître, *et al.*, "Measuring topological invariants from generalized edge states in polaritonic quasicrystals", *Physical Review B*, vol. 95, no. 16, 2017, ISSN: 24699969. DOI: 10.1103/PhysRevB.95.161114.

[15] G. Rai, H. Schlömer, C. Matsumura, S. Haas, and A. Jagannathan, "Bulk topological signatures of a quasicrystal", *Physical Review B*, vol. 104, no. 18, 2021, ISSN: 24699969. DOI: 10.1103/PhysRevB.104.184202.

[16] N. Macé, A. Jagannathan, P. Kalugin, R. Mosseri, and F. Piéchon, "Critical eigenstates and their properties in one- and two-dimensional quasicrystals", *Physical Review B*, vol. 96, no. 4, 2017, ISSN: 24699969. DOI: 10.1103/PhysRevB.96.045138.

[17] P. Kalugin and A. Katz, "Electrons in deterministic quasicrystalline potentials and hidden conserved quantities", *Journal of Physics A: Mathematical and Theoretical*, no. 31, 2014, ISSN: 17518121. DOI: 10.1088/1751-8113/47/31/315206.

[18] M. Tinkham, *Introduction to superconductivity*, 2nd ed. Dover Publications Inc., 2004, ISBN: 9780486435039.

[19] J. Bardeen, L. N. Cooper, and J. R. Schrieffer, "Microscopic theory of superconductivity", *Physical Review*, vol. 106, no. 1, 1957, ISSN: 0031899X. DOI: 10.1103/PhysRev.106.162.

[20] J. Bardeen, L. N. Cooper, and J. R. Schrieffer, "Theory of superconductivity", *Physical Review*, vol. 108, no. 5, 1957, ISSN: 0031899X. DOI: 10.1103/PhysRev.108.1175.

[21] C. Timm, *Lecture notes: Theory of Superconductivity*. TU Dresden, Institute of Theoretical Physics, 2020. [Online]. Available: https://tu-dresden.de/mn/physik/itp/cmt/ressourcen/dateien/skripte/Skript_Supra.pdf?lang=en (visited on Sep. 8, 2022).

[22] J.-X. Zhu, *Bogoliubov-de Gennes Method and Its Applications*. Cham: Springer International Publishing, 2016, vol. 924, ISBN: 978-3-319-31312-2. DOI: 10.1007/978-3-319-31314-6.

[23] N. W. Wennerdal, A. Ask, P. Holmvall, T. Lofwander, and M. Fogelstrom, "Breaking time-reversal and translational symmetry at edges of d -wave superconductors: Microscopic theory and comparison with quasiclassical theory", *Physical Review Research*, vol. 2, no. 4, 2020, ISSN: 26431564. DOI: 10.1103/PhysRevResearch.2.043198.

[24] B. T. Polyak, "Some methods of speeding up the convergence of iteration methods", *USSR Computational Mathematics and Mathematical Physics*, vol. 4, no. 5, 1964, ISSN: 00415553. DOI: 10.1016/0041-5553(64)90137-5.

[25] A. Zagoskin, *Quantum Theory of Many-Body Systems*. Cham: Springer International Publishing, 2014, ISBN: 978-3-319-07048-3. DOI: 10.1007/978-3-319-07049-0.

[26] A. F. Andreev, "The thermal conductivity of the intermediate state in superconductors.", *Sov. Phys. JETP*, vol. 19, no. 5, p. 1228, 1964.

[27] I. Kulik, "Macroscopic quantization and the proximity effect in s-n-s junctions", *Sov. Phys. JETP*, vol. 30, no. 5, p. 944, 1970.

[28] K. K. Likharev, "Superconducting weak links", *Reviews of Modern Physics*, vol. 51, no. 1, pp. 101–159, Jan. 1979, ISSN: 0034-6861. DOI: 10.1103/RevModPhys.51.101.

[29] C. W. J. Beenakker, "Three "Universal" Mesoscopic Josephson Effects", in *Transport Phenomena in Mesoscopic Systems*, Springer Berlin Heidelberg, 1992, pp. 235–253. DOI: 10.1007/978-3-642-84818-6{_}22.